ON THE ANTIFERROMAGNETIC RESONANCE IN $CuCl_2 . 2H_2O$

H. J. GERRITSEN

ON THE ANTIFERROMAGNETIC RESONANCE IN $CuCl_2.2H_2O$

PROEFSCHRIFT

TER VERKRIJGING VAN DE GRAAD VAN DOCTOR IN DE WIS- EN NATUURKUNDE AAN DE RIJKSUNIVERSITEIT TE LEIDEN OP GEZAG VAN DE RECTOR MAGNIFICUS DR A. E. VAN ARKEL, HOOGLERAAR IN DE FACULTEIT DER WIS- EN NATUURKUNDE. PUBLIEK TE VERDEDIGEN OP WOENSDAG 26 OCTOBER 1955. TE 14 UUR

DOOR

HENDRIK JURJEN GERRITSEN
GEBOREN TE DEN HAAG IN 1927

UITGEVERIJ EXCELSIOR - ORANJEPLEIN 96 - 'S-GRAVENHAGE

Promotor: Prof. Dr C. J. Gorter

Aan mijn Vader en Moeder

Aan mijn Vrouw

VOORWOORD

Teneinde te voldoen aan de wens van de Faculteit der Wis- en Natuurkunde volgt hier een korte schets van mijn academische studie.

In Juli 1945 begon ik mijn studie in de natuur- en scheikunde te Leiden. Hier legde ik in November 1948 het candidaatsexamen letter E af. Na nog enige maanden op het Kamerlingh Onnes laboratorium gewerkt te hebben bij Dr.G.J.van den Berg, werd ik opgeroepen voor het vervullen der militaire dienstplicht.

Het laatste halfjaar van de dienstperiode bracht ik door op het physisch laboratorium der rijksverdedigingsorganisatie onder leiding van Prof.Dr.Ir.J.L.van Soest. Een deel van het physisch-chemisch werk dat ik daar verrichtte, kon ik later gebruiken voor het doctoraal tentamen physische chemie bij Prof.Dr.C.J.F.Böttcher.

Toen ik in Juli 1950 de dienst met groot verlof verlaten kon, zette ik mijn studie op het Kamerlingh Onnes laboratorium voort. Spoedig kreeg ik een aanstelling als assistent en kwam ik te werken in de groep die zich bezig houdt met microgolf-experimenten onder leiding van Prof.Dr.C.J.Gorter. Hier werkte ik samen met J.Ubbink en J.A.Poulis, terwijl ik mij voorbereidde voor het doctoraalexamen in de experimentele natuurkunde en daartoe de colleges volgde van wijlen Prof.Dr.H.A.Kramers en Dr.J.Korringa (thans werkzaam te Ohio).

In Juni 1952 legde ik het doctoraalexamen af. Van veel nut voor mijn theoretische vorming was de door Dr.P.H.E.Meijer en Dr.J.Korringa geleide werkgroep voor paramagnetisme, waaraan ik actief deel nam.

Na enige paramagnetische resonantie metingen verricht te hebben, o.a. aan vrije radicalen, concentreerde ik mijn aandacht op de antiferromagnetische resonantie. Na de promotie van J.Ubbink in Maart 1953, heb ik samengewerkt met: R.Okkes, B.Bölger, G.W.J. Drewes en K.van Damme. Het laatste jaar heb ik nauw samengewerkt met Dr.M.Garber van de universiteit van Illinois en in samenwerking met hem zijn de meeste onderzoekingen van dit proefschrift tot stand gekomen.

Tijdens mijn werkzaamheden op het Kamerlingh Onnes laboratorium heb ik, behalve van de wetenschappelijke staf, ook veel lering en steun mogen ontvangen van de technische- en administratieve staf.

CONTENTS

INTRODUCTION

In magnetic substances interactions exist between the magnetic moments. In some cases these interactions tend to align the magnetic moments all in the same direction (ferromagnetism), and in other cases they tend to surround each magnetic moment by neighbouring magnetic moments of antiparallel alignment (antiferromagnetism). One of the possible structures in which the latter tendency is realized, is in a lattice that consists of two interlocking sublattices while the magnetic moments in each of the sublattices have the same direction, but the two directions for the two sublattices are antiparallel to each other.

These interactions, that try to create a magnetic long range order, are counteracted by thermal agitation and if this agitation is too strong, no long range order will exist. There is a certain temperature below which the interactions give rise to ferromagnetism or antiferromagnetism and above which the substance behaves paramagnetically. This critical temperature is called the Néel temperature in the case of antiferromagnetism.

For copperchloride dihydrate this temperature equals $4.3^{\circ}K$. When at a temperature where the substance behaves paramagnetically a static magnetic field, H, is applied, it is a well known property that the magnetic moments start precessing around this field with a circular frequency ω, the Larmor frequency, defined by: $\omega = \gamma H$.

High frequency radiation energy of the same frequency ω, will be absorbed by the precessing spin-system.

When the same experiment is done at a temperature where the substance is antiferromagnetic, there is again a relation between the resonance frequency ω and the static field H. Based on the model of Gorter and Haantjes [5] for antiferromagnetism, Ubbink could derive this relation for the antiferromagnetic resonance. The theory could give a good explanation of the experiments [1, 2, 3, 4]. At the same time Nagamiya and Yosida [6,7] developed theories, which – although their assumptions were different from those of Gorter, Haantjes and Ubbink – were also applicable to this case.

The resonance frequency ω, is no longer connected with H by a simple linear relation, as was the case for paramagnetic resonance. This is due to the fact, that in antiferromagnetism one has to consider the motion of two antiparallely directed spins together, under the influence of the static magnetic field and their own mutual interaction forces. This is a much more complicated problem, as is the case for paramagnetic resonance where

one single spin is considered and the interaction with other spins is assumed to be small with respect to the interaction with the static magnetic field.

The purpose of the investigations collected in this thesis, was to extend the existing measurements and to develop the theory, based on the classical picture of the molecular field, as far as possible.

In this respect measurements have been done at very high frequencues (chapter I) and the results have been explained by applying Ubbink and Yosida's theories to that case (chapter II).

A new feature has been added to their theories, namely that resonance absorption has to be expected when the static field is applied in the *ac*-plane and has a value, characterized by the threshold hyperbola of Gorter and Haantjes [5]. The spin-system has no well defined orientation in this case; when H is slightly smaller than the value of the hyperbola, the spin-system is oriented in the *ac*-plane, but when H is slightly greater than the value of the threshold hyperbola, the spin-system stays perpendicular to the *ac*-plane. The orientations in between correspond to a range of resonance frequencies. This resonance has been observed in the experiments, thus giving a direct determination of the threshold hyperbola.

In chapter III a detailed study of the resonance diagram in the *ab*-plane at 9500 MHz. was made and it was found that minor discrepancies occurred between the experiment and the theory.

Experiments at 9400 MHz. on the intensity of the resonance-absorption are described and the design of a new cavity, developed for this study, is given in chapter IV.

In chapter V linewidth measurements at 9400 MHz. are described, together with a method for accurately measuring narrow resonance lines.

No theory existed for the experiments of Ch. IV and a theory has been developed in chapter VI. This theory of the antiferromagnetic rotator is based on the introduction of a h.f. magnetic field, that is introduced as a perturbation on the static field, and on the introduction of damping terms in the equation of motion, analoguous as has been done by F.Bloch for the paramagnetic case.

It was possible to account for the observed intensities with this theory.

A summary of the search for new substancies that would show antiferromagnetic resonance is given in chapter VII and one of them, manganese bromide tetrahydrate, proved to be interesting for a further study.

Chapter I

ANTIFERROMAGNETIC RESONANCE IN HYDRATED COPPER CHLORIDE AT 32000 MHz

1. Experimental method

The apparatus consisted of a microwave spectrometer with a cavity operated in the TE_{011} mode, used in transmission. The transmitted energy was detected by means of a crystal connected to a galvanometer. The klystron used was generously placed at our disposal by Dr R.A. Smith and Dr F.E. Jones of the Telecommunication Research Establishment, Malvern, Great Britain. The klystron frequency was adjusted manually at the top of the cavity resonance. Using field modulation the absorption curve could also be displayed on a cathode ray oscilloscope. The cavity was connected to German silver wave guides which were sealed vacuum tight at the room temperature side by ½ λ-polystyrene windows.

Liquid helium was allowed to enter the cavity in order to guarantee a well defined homogeneous temperature. The increase of noise due to vapour bubbles in the cavity disappears below the lambda temperature. The crystal was placed in the middle of the cavity, where the high frequency magnetic field is vertical and the electric field is zero. The static magnetic field rotated in a horizontal plane and thus remained perpendicular to the high frequency magnetic field.

The volume of the copper chloride crystals was about 1 mm^3. In the cutting and in the adjusting of the crystals a polarization microscope was a great help. Making use of the pleochroism of the crystal it was even possible to distinguish between the *b*-axis of the crystal and the other two axes. The transmitted light was blue when it was polarized along the *b*-axis and green-yellow when polarised along the *a*- or *c*-axis. The *c*-axis is easily recognized since the crystals grow in that direction. The error in the orientation of the crystals was at most 5° in the most unfavourable cases (*ac*-crystals with the *b*-axis vertical). The adjustment of the crystals in the cavity was controlled by observing the paramagnetic resonance at room temperature. The frequency was derived from the narrow paramagnetic resonance line of a small amount of diphenyl trinitrophenyl hydrazine inserted in the cavity. The magnetic field was calibrated with the help of proton magnetic resonance. Usually the resonances were observed on the screen of the oscilloscope while the magnetic field was modulated with 50

c.p.s. In the study of the linewidths, however, the slower galvanometer method was used in order to avoid errors due to anomalous dispersion.

An important element in the detector circuit was the specially designed input transformer of the audio amplifier which kept the noise figure low.

The electromagnet used, which had been constructed by Prof. F. Zernike, was kindly placed at our disposal by Prof. H. Brinkman at the University of Groningen. It was provided with pole pieces of 14 cm diameter in order to avoid variations in the magnitude of the field when it was rotated.

2. Experimental results

A. *Results obtained in the paramagnetic state*

Assuming the g-factor of the diphenyl trinitrophenyl hydrazine sample to be 2.0038 [9] the values for g in the a, b and c directions were determined. They were the same at liquid air temperatures (80°K) and at liquid hydrogen temperatures (20°K). In Table I they are compared with those derived by Itoh, Fujimoto and Ibamoto [10] from observations at 9400 MHz and those derived from susceptibility measurements by Van den Handel, Gijsman and Poulis [11].

Table I

Frequency	g_a	g_b	g_c
32000 MHz	2.187	2.037	2.252
9400 MHz [10]	2.195	2.075	2.26
suscept. [11]	2.18	2.03	2.24

I suppose the high g_b value given by Itoh *et al.* to be in error.

The linewidth proved equally to be the same at 80°K and at 20°K. The width between points of half absorption was 130 Ø when the field was along the a-axis and 85 Ø when along the b-axis. At 4.33°K, just above the temperature where antiferromagnetism sets in, a tail has developed at the high field side. This leads to widths of 300 Ø and 200 Ø in the directions of the a- and b-axes respectively (see fig. 1*a*, *b*, *c*).

B. *Results obtained in the antiferromagnetic state*

Two kinds of crystals have been investigated: ab-crystals in which the c-axis was oriented vertically and ac-crystals in which

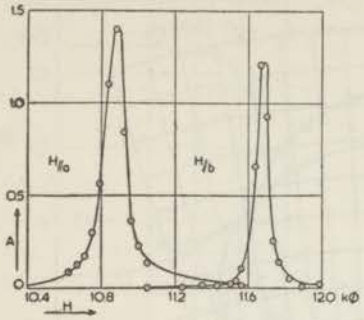

Fig. 1a. Line shapes of the paramagnetic resonance at 20°K.

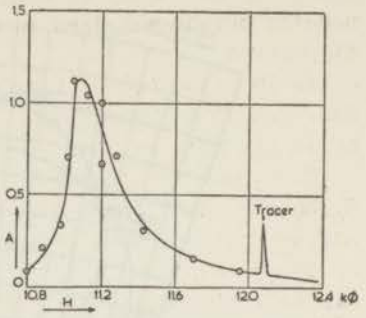

Fig. 1b. Absorption curve at 4.33°K with H along the a-axis.

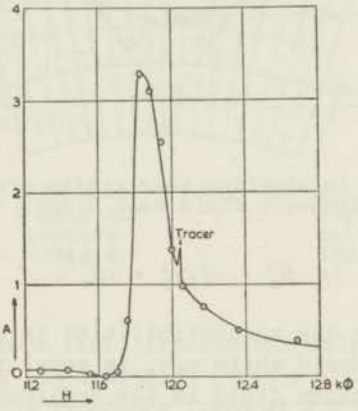

Fig. 1c. Absorption curve at 4.33°K with H along the b-axis.

the b-axis was vertical. The direction of the static field could be varied in the horizontal plane. The results are displayed in the diagrams 2, 5 and 4 which show the resonance fields for different angles in the ab-plane near the a- and b-axes and in the ac-plane near the a-axis.

a-direction. The case where the field was in the a-direction was especially studied in an ac-crystal as a function of the temperature. In general three antiferromagnetic resonance fields were found as is shown in fig. 3a. The highest one gradually merges into the paramagnetic resonance upon approaching the Néel temperature. According to theory this resonance field H_x is connected to the threshold field H_c^* and the anisotropy parameter

$$\alpha = 1 - g_b^2 \chi_a / g_a^2 \chi_b$$

at the temperature considered by the relation

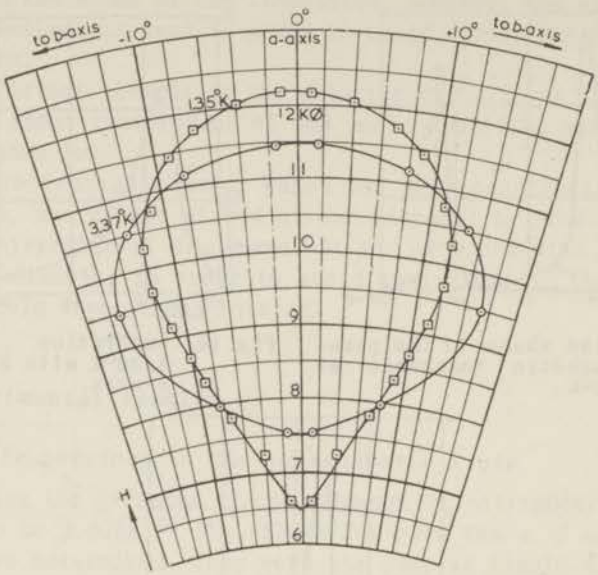

Fig. 2. H in ab-plane near a-axis. Free radical resonance field was: 11280 Φ = ω/γ.

$$H_x^2 = \omega^2/\gamma_a^2 + \alpha H_c^{*2}. \qquad (1)$$

Here χ_a and χ_b are the susceptibilities in small fields at the temperature considered while ω/γ_a is equal to the value of the paramagnetic resonance field in the a-direction. The values of αH_c^{*2} obtained from this formula and of α derived by applying also the well known values of H_c^* (see following sentence) are marked by circles in the figures 6 and 7.

The middle resonance field was only observed below 4.0°K. In accordance with theory its value agrees within 0.5% with the threshold field H_c^* observed by the proton resonance method *) [12] of Poulis and Hardeman. Our resonance field values are about 40 Φ below their H_c^* curve. It is uncertain if this is a real effect, as its magnitude is just of the order of the error in the magnetic field readings due to hysterese in the iron of the pole pieces. At the lowest temperature (1.35°K) this absorption peak had a width of only 15 Φ but its wings were rather broad. The intensity of the absorption was weak in the a-direction, but increased rapidly when the field was rotated a few degrees towards the b- or c-directions. At 3°K the halfwidth had doubled and it increased rapidly with further rise in temperature. When the field was rotated towards the c-axis, the threshold hyperbola in the ac-plane was found.

*) A few minor corrections however have to be applied to the published data, which lower their curve by 0.1%.

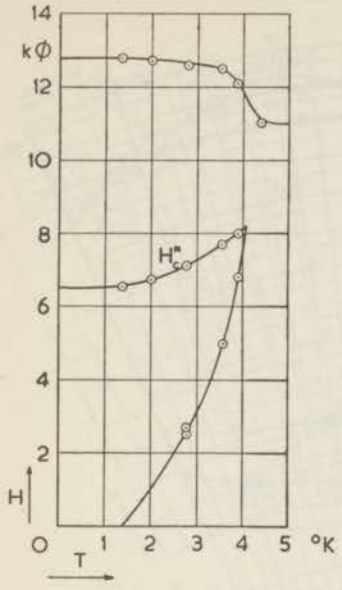

Fig. 3a. Resonance fields with H along the a-axis at different temperatures; ω/γ = 12050 Φ.

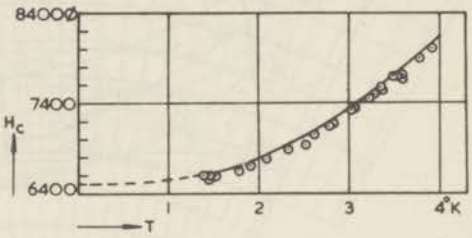

Fig. 3b. Resonance fields compared with the threshold field versus temperature curve of [12]).

The lowest resonance field finally was only observed between about 2.7°K and 4.0°K. It increases rapidly with the temperature, merging into the middle resonance field at 4.0°K above which temperature both resonances vanish. It may be remarked that this resonance was observed along all directions in the ac-plane. At 3.55°K e.g. the resonance field along the a-axis is 5000 Φ and goes to 6900 Φ when H is along the c-axis (not visible in the diagram).

b-direction. In fields along the b-direction one antiferromagnetic resonance line was observed. In the temperature region at about 2.7°K the Q-factor of the cavity was found to be very low and neither an antiferromagnetic resonance nor the paramagnetic resonance of the free radical sample could be detected. Studying fig. 5 it is seen that just at this temperature the hyperboloid resonance curves in the ab-plane rapidly change their character, the b-axis apparently behaving there as a degeneracy of the curves. From the relation

$$H_y^2 = \omega^2/\gamma_b^2 - g_a^2 \alpha H_c^{*2}/g_b^2 \qquad (2)$$

one may derive another set of αH_c^{*2}-values and, making use of the known H_c^*, also of the α-values. The results are marked by trian-

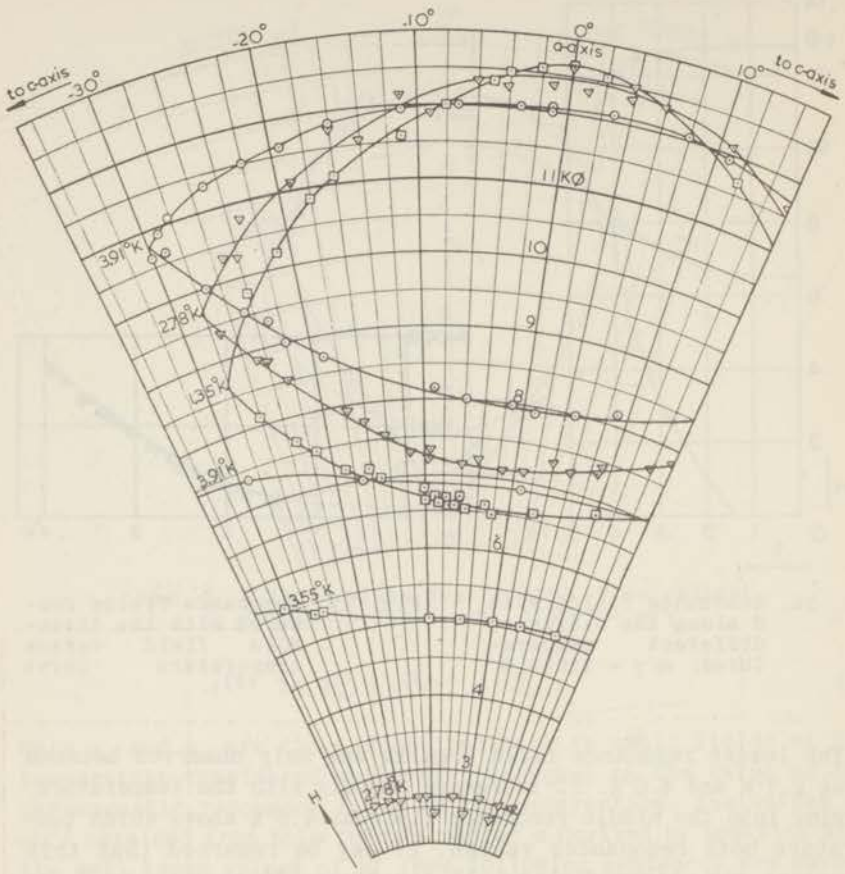

Fig. 4. H in ac-plane near a-axis.

ω/γ	T
12100 Φ	3.91°K
12090 Φ	3.55°K
12020 Φ	2.78°K
11910 Φ	1.35°K

gles in the figures 6 and 7. On the whole the agreement with the set obtained from (1) is satisfactory, though there may be a small systematic difference.

It must be mentioned that, especially with one ac-crystal, a resonance field of paramagnetic character was observed at all temperatures. A similar phenomenon was also found in some of the earlier 9400 MHz investigations. One is inclined to ascribe it to the beginning of deterioration of the crystal.

The rather broad frequency band of the klystron made it possible to carry out experiments at somewhat different frequencies. In fig. 8 the resonance curves for two slightly different fre-

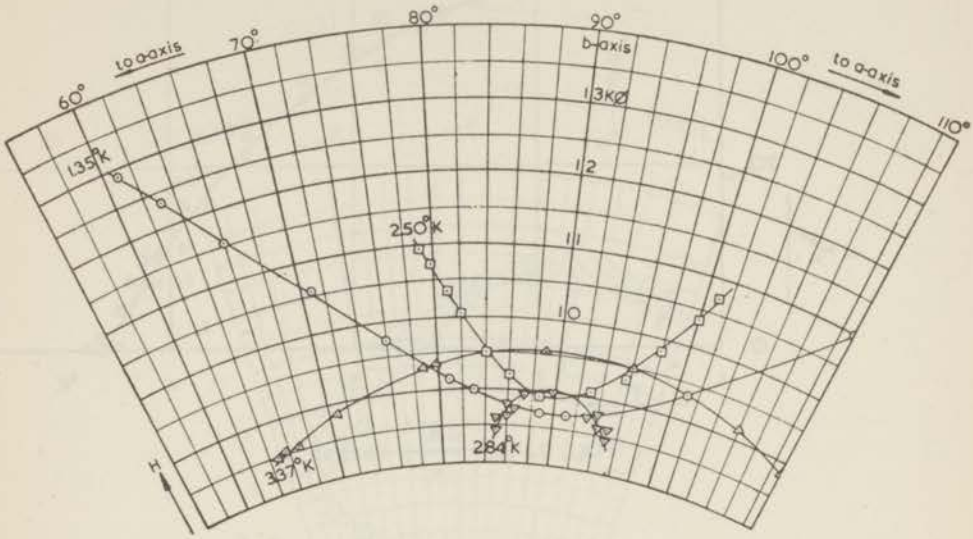

Fig. 5. H in ab-plane near b-axis; ω/γ = 11280 Φ

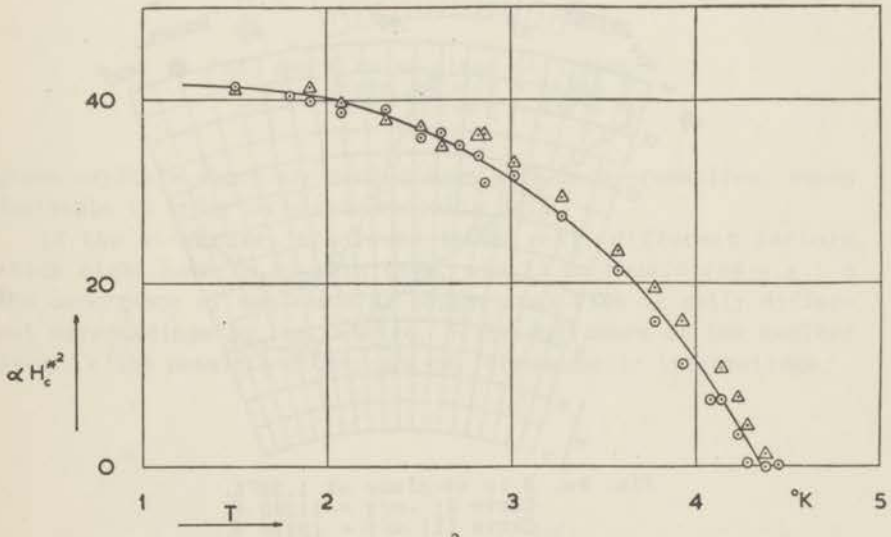

Fig. 6. αH_c^{*2} versus T.

quencies are given in the ab- and the ac-plane. It is clear that the resonance curve coinciding with the threshold hyperbola is not affected by the change in frequency.

Below a temperature of about 2.5°K structures in the central part of certain resonance bands were observed on the oscilloscope screen while also weak resonances at a distance of the order of 150 Φ from the main resonances appeared.

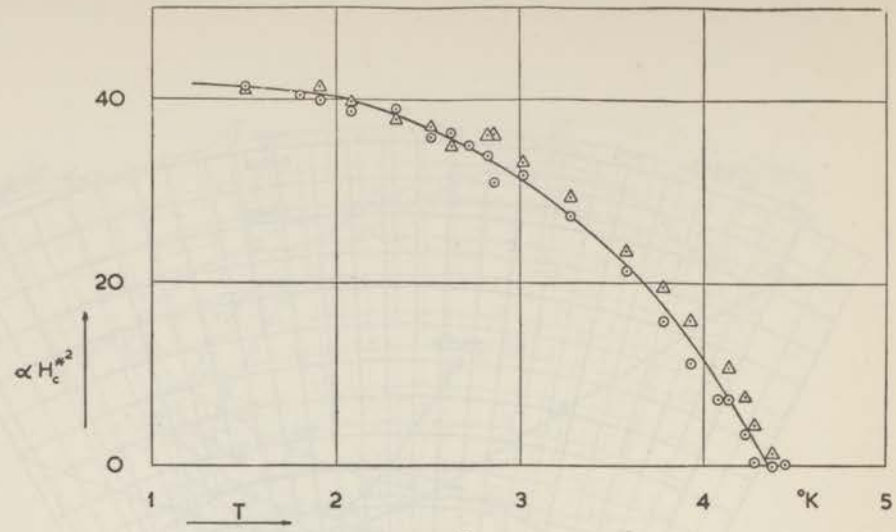

Fig. 7. $\alpha = \frac{\alpha H_c^{*2}}{H_c^{*2}}$ versus T.

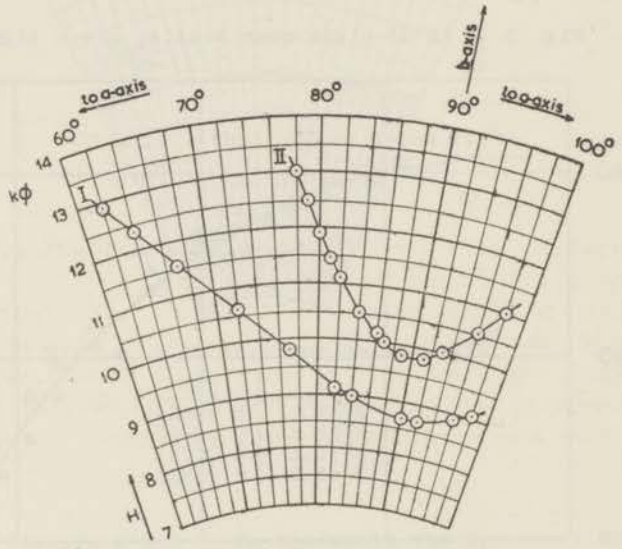

Fig. 8a. H in ab-plane at 1.35°K.
Curve I: ω/γ = 11280 Φ.
Curve II: ω/γ = 12110 Φ.

When the field was along the a-axis the structures were apparent in the highest of the three resonance bands but not in the sharp peak at the threshold field. In this case, as well as in the case where the field was along the b-axis, a partial decomposition into three lines with mutual separations of about 35 Φ was observed. The character of the structures, however, was not quite the same in different crystals so that a further study on well

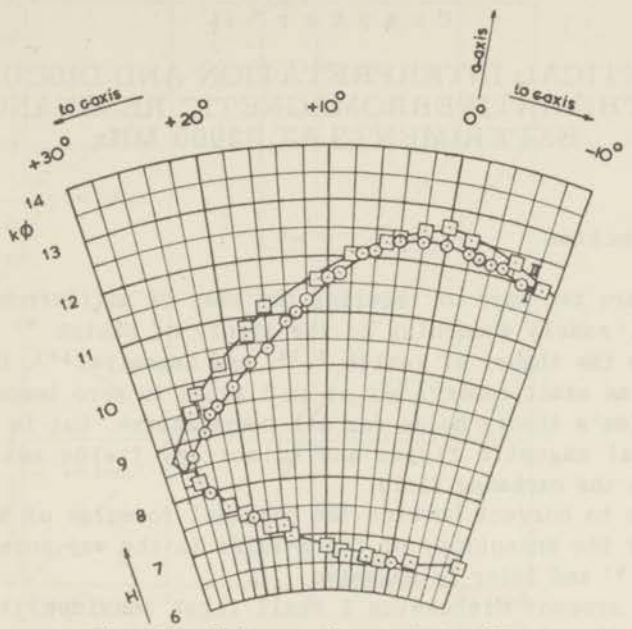

Fig. 8b. H in ac-plane at 1.35°K.
Curve I: ω/γ = 11380 Φ.
Curve II: ω/γ = 11910 Φ.

grown crystals which are cooled down with much precaution, seems desirable in order to obtain reliable data.

If the structures are found to be real, different factors which might have to do with them, should be considered e.g.: *a* the occurrence of two kinds of copper ions with slightly different surroundings in the lattice, *b* the influence of the nuclear spins, *c* the possible occurrence of ferromagnetic interactions.

Chapter II

THEORETICAL INTERPRETATION AND DISCUSSION ON THE ANTIFERROMAGNETIC RESONANCE EXPERIMENTS AT 32000 MHz

1. Introduction

There are two ways of treating the case of antiferromagnetic resonance, namely according to the theory of Ubbink [4] or according to the theory of Yosida [6][16] and Nagamiya [17]. Ubbink's theory is an exact theory, but it is limited to zero temperature, while Yosida's theory holds for all temperatures, but is limited to external magnetic fields and anisotropy fields small with respect to the exchange field.

One has to correct however the original formulae of Yosida's theory for the anisotropy of the g-value in the way pointed out by Ubbink [4] and later by Nagamiya [7].

In the present discussion I shall first consider the case where both theories give the same result, namely, at zero temperature, and simplify Ubbink's equations by supposing the external field and the anisotropy field to be small compared with the exchange field.

This simplification is not essential, but gives a considerable reduction of the work on the calculations. It may be remarked that the resonance fields are of the order of 5 per cent of the exchange field at 0°K. Effects due to this simplification are not likely to be observable in the lower temperature range, since they enter into the formulae as squares of that 5 percent, while experimental errors due to misalignments of the crystals and the width of the resonance lines reduce the possibility of measuring such small effects.

2. Extrapolation to zero temperature

A. *Crystal axes*

The result of calculations of the resonance frequencies along the three crystal axes has been given in fig. 1, 2 and 3; all the diagrams are for zero temperature.

ω/γ_x is plotted vertically, being the magnetic field H_{px} corresponding to paramagnetic resonance in copper chloride with the external magnetic field along the a-axis. This value is obtained

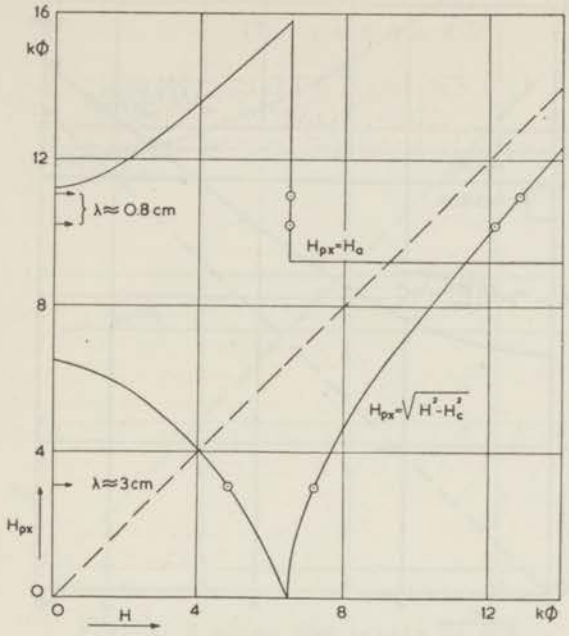

Fig. 1. H along the a-axis at 0°K.

from the resonance field of the paramagnetic tracer: diphenyl trinitrophenyl hydrazine, multiplying this field by the ratio of the g-values:

$$\omega/\gamma_x = H_{px} = H_{tracer}\ 2.004/2.187.$$

The dotted line represents the resonance to be expected if the copper chloride would remain paramagnetic.

The arrows in the figures indicate the position of the 3 cm experiments: ω/γ_x = 3100 Φ giving only resonance lines when H is along the a-axis, and the 8-9 mm experiments with ω/γ between 10200 Φ and 11100 Φ.

If the symmetry is not rhombic but unaxial, the result is to be found by replacing H_a by 0 and H_b by H_c. This leads to the formulae derived by Kittel [15]. Then the resonance frequencies for $H < H_c$ along the a-axis are: $\omega_{1,2} = \gamma(H_c \pm H)$.

Keffer, Kaplan and Jafett [18] have discussed the normal modes in these two cases. Angular frequencies with the + sign have the same sense of precession as a paramagnetic magnetic moment and the angular frequencies with the − sign have the opposite sense of precession as occurs in paramagnetic resonance.

This remains true for the two branches for $H < H_c$ in fig. 1,

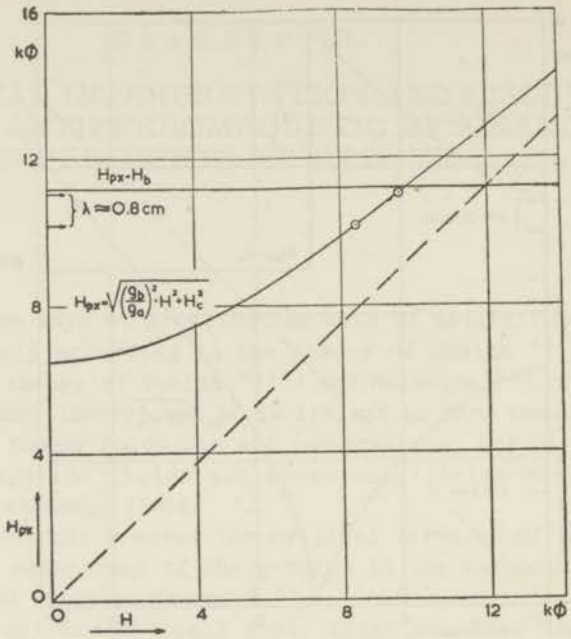

Fig. 2. H along the b-axis at 0^{o}K.

although now the precession is in an ellipse, instead of in a circle. See further chapter VI.

In the 8 mm experiments one of the resonances along the a-axis takes place at the critical field $H = H_c$. At that fieldstrength the direction of the spins in the ab-plane is undetermined. For spins along the a-axis the resonance occurs at: $H_{px} = \sqrt{H_b^2 + 3H_c^2}$ as follows from Ubbink's equation (4) and for spins along the b-axis at $H_{px} = H_a$. See fig. 1. Intermediate orientations of the spins correspond to frequencies lying between these two extrema. Nagamiya also stressed this point and called this phenomenon: "orientation resonance". An error in his calculations, however, made him overlook the simple physical meaning of these frequencies, see for example ref. [5], fig. 11, namely that they play the role of "missing link" in the frequencies between fields lower and higher than H_c. The higher root for $\psi = 0$ should be in his notation: $-C_1 + C_2 + (C_1/\alpha)(1 + \alpha)^2$. The occurrence of these missing link frequencies also appears in Ubbink's picture, ref.[4], fig. 4.

Before considering the case of resonance along the axes at finite temperatures, the equations (4) and (5) of Ubbink [4] will be examined in order to see what happens in the coordinate planes.

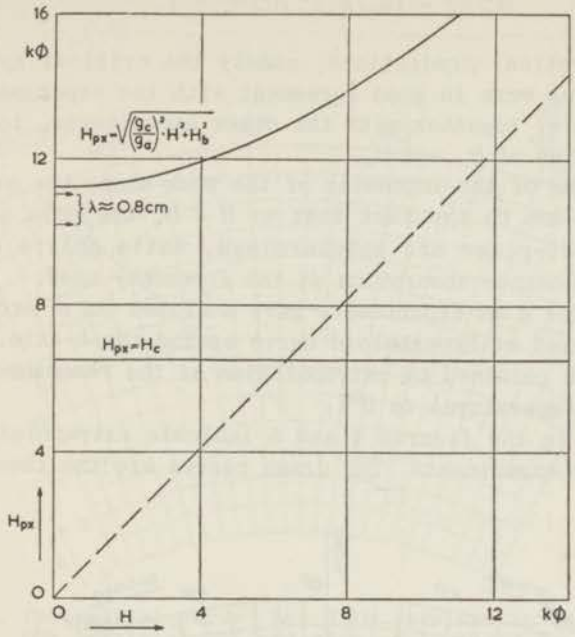

Fig. 3. H along the c-axis at $0^{\circ}K$.

B. *Coordinate planes*

ac-plane. Here one of the solutions is the critical hyperbola, this being a general kind of orientation resonance. The easiest way to prove this is by calculating the resonance lines for $H < H_c$ and for $H > H_c$. For $H < H_c$ two curves of the 4th degree are found. The lowest one of these was observed in the 3 cm experiments by Ubbink *et al.* [2]. The upper branch is imaginary when $H_{px} < H_b$ as is the case in the 8 mm experiments for $T = 0^{\circ}K$.

For $H > H_c$ the resonance curve is:

$$\frac{H_x^2}{H_c^2 + H_{px}^2} - \left(\frac{g_c}{g_a}\right)^2 \frac{H_z^2}{H_a^2 - H_{px}^2} = 1 ,$$

(formula 5 of Ubbink [4]).

Here the spins are orientated along the b-axis. When $H_{px} = 3100\ \Phi$ this resonance curve is a hyperbola because $H_{px} < H_a$. When H_{px} is greater than H_a, as is the case in the 8 mm experiments, the resonance curve is an ellipse. When $H_{px} = H_a$ the resonance diagram in the *ac*-plane degenerates into a single straight line along the a-axis. One should therefore expect that the *ac*-plane ellipse is tninner the closer H_{px} gets to H_a.

This is shown in fig. 8b of chapter I. The lower part of the resonance curve is in both cases the same namely the critical hyperbola of Gorter and Haantjes:

$$H_x^2/H_c^2 - (g_c/g_a)^2 H_z^2/H_a^2 = 1.$$

These theoretical predictions, namely the critical hyperbola and the ellipse, were in good agreement with the experiments and made it possible, together with the other experiments, to obtain an accurate value of H_c and H_a.

The smallness of the intensity of the peak along the a-axis at $H = H_c$ may be due to the fact that at $H = H_c$ the spin orientations in the ab-plane are undetermined, while only a certain angle gives resonance absorption at the frequency used.

ab-plane. The 8 mm experiments gave a closed curve around the a-axis and a kind of hyperboloid curve around the b-axis. Curves at $T = 0^oK$ were obtained by extrapolation of the resonance graphs at different temperatures to 0^oK.

The points in the figures 4 and 5 indicate extrapolations to $T = 0^oK$ of the experiments. The drawn curves are the theoretical curves.

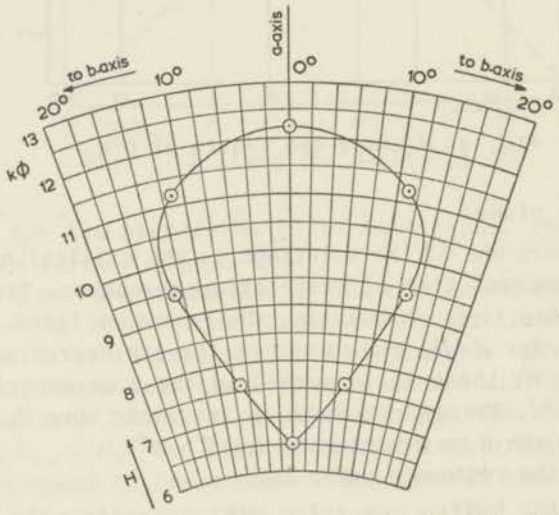

Fig. 4. Theoretical curves for H in ab-plane in the region of the a-axis at 0^oK and with $\omega/\gamma = 11280$ Φ.

The equation determining the curves is:

$$0 = Z^3 - Z^2(H'^2 + H_{px}^2 + H_c^2 - 2H_b^2) +$$
$$+ ZH_{px}^2(-3H'^2 + 2H_{px}^2 + H_c^2 - 2H_b^2) + 2H_{px}^2(H'^4 - H_c^4).$$

See Ubbink: formulae (6), (7), (8), (9) [4].

A more rapid way to calculate the theoretical curves was used than Ubbink did, one of whose steps was to solve Z as a root of the third degree equation.

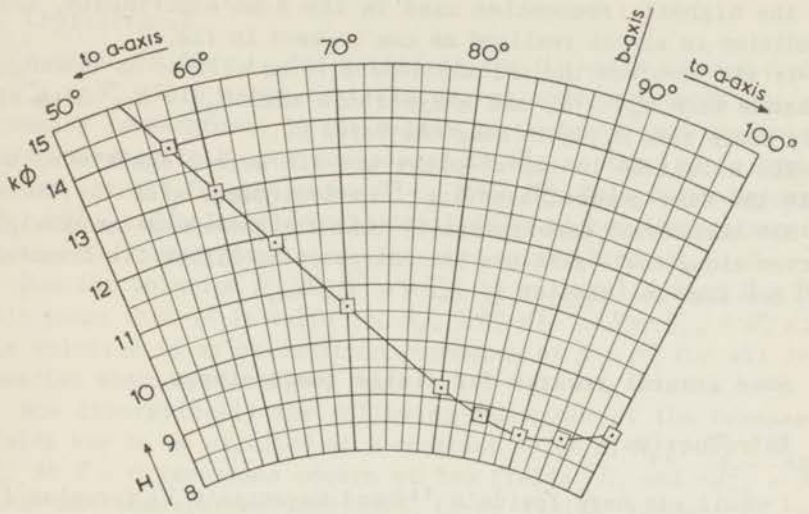

Fig. 5. Theoretical curve for H in ab-plane in the region of the b-axis at 0°K and with ω/γ 11280 Φ.
□ are the extrapolated experimental points.

If one takes $H'^2 = Z + pH_c^2$, in which p is a parameter, then the Z^3 term cancels out when putting this H'^2 in the formula. This gives a quadratic equation in Z.

Z is defined by: $Z^2 = H_c^4 + H'^4 - 2H_c^2H'^2 \cos 2\theta$, and

$$H_{exp} = \frac{H'}{\sqrt{\cos^2\theta + \left(\frac{g_b}{g_a}\right)^2 \sin^2\theta}}$$

Special cases: $\theta = 0^o$ gives: $H'^2 = H_x^2 = Z + H_c^2$. The roots of the quadratic equation are: $Z = 0$ and $Z = H_{px}^2$. This gives: $H_x = H_c$ and $H_x = \sqrt{H_{px}^2 + H_c^2}$ as was expected. Variation of p between 1 and 0.8 gives Z, H' and θ and gave the drawn curve in fig. 4, resembling a kite. $\theta = 90^o$ gives: $H'^2 = Z - H_c^2$ with $Z = H_{px}^2$ and thus:

$$\left(\frac{g_b}{g_a}\right)^2 H_y^2 = H_{px}^2 - H_c^2 .$$

Variation of p between -1 and -½ gives the theoretical curve, drawn in fig. 5.

Both "kite" and hyperboloid curve are in perfect accordance with the experimental points when extrapolated to $T = 0$ if one takes in the theoretical curves: H_c = 6500 Φ and H_b = 11200 Φ (so that $H_a = \sqrt{H_b^2 - H_c^2}$ = 9100 Φ)

The hyperboloid curve along the b-axis deserved some more attention.

A straight line should be expected when $H_{px} = H_b$ (see fig. 2). At the highest frequencies used in the 8 mm experiments, this condition is almost realised as can be seen in fig. 2.

In the bc-plane the calculations give an ellipse as resonance diagram when $H_{px} > H_b$ and a hyperbola when $H_{px} < H_b$. Both are very sharp when H_{px} gets near the value H_b.

The solutions in the ab-plane are 4th degree equations, but with the same general behaviour. In accordance with the theory it has been found experimentally that the resonance hyperboloid curves along the b-axis are the sharper, the higher the frequency is. See fig. 8a, chapter I, for $T = 1,3^{\circ}K$.

3. Some general remarks for finite temperatures

A. *Introduction*

I shall use here Yosida's [16] and Nagamiya's [7] formulae for a few simple cases, namely: H along the crystal axes and for H in the ac-plane.

Although the basic idea in this theory is that the spins of the two sublattices are supposed to be strictly antiparallel, it is found that even at temperatures near the Néel point, where the anisotropy energy and the magnetic energy should lead to an appreciable amount of deviation from antiparallelity, the theory gives a good agreement with the experiments.

The treatment of Yosida and Nagamiya leads to a formalism which is very similar to that used by Gorter, Haantjes and Ubbink at $T = 0$. The role of H_c, H_a and H_b is taken over by other fields, which we shall call H_c^*, H_a^* and H_b^* and which at $T = 0$ are equal to H_c, H_a and H_b. An other important quantity is $\alpha = 1 - \chi_{\parallel}/\chi_{\perp}$, where $\chi_{\parallel} = \chi_{aa}$ and $\chi_{\perp} = \chi_{ab}$. See Ubbink, ref. [4], formula (16).

The symbols used by Yosida and Nagamiya are connected to those used by us by:

$$2AK_1 = \alpha H_c^{*2} . (g_a/2)^2$$

$$2AK_2 = \alpha H_b^{*2} . (g_a/2)^2$$

$$|\omega/\gamma_x| = H_{px} .$$

See also chapter VI, where a table is given for reference.

It will be assumed with Nagamiya and Yosida that the temperature dependence of H_a^*, H_b^*, H_c^* is the same and use $H_c^*(T)$ for that.

Evidence for that is found experimentally in the ac-plane ellipses (see later). I will use the αH_c^{*2}- and α-curves of chapter I.

B. *Crystal axes*

a-axis. In fig. 1, the points at the H_{px}-axis become: $\sqrt{\alpha}H_b^*$; $\sqrt{\alpha}H_a^*$; $\sqrt{\alpha}H_c^*$. This means that the curves move downwards with increasing temperature. On the H-axis it is found that the points corresponding to H_c now correspond to H_c^*, so they go to higher values, except for the curve $H_{px}^2 = H^2 - H_c^2$. This curve becomes: $H_{px}^2 = H^2 - \alpha H_c^{*2}$. It will go to the left at higher temperature and at the Néel temperature merge into the dotted line: $H_{px} = H$.

Now the solution $H_{px}^2 = H^2 - \alpha H_c^{*2}$ is only valid when $H \geq H_c^*$. This means that it is valid for $H_{px} \geq H_c^* \sqrt{1-\alpha}$. For $H_{px} < H_c^* \sqrt{1-\alpha}$ the solution is an orientation resonance at $H = H_c^*$ for all frequencies where $\omega/\gamma_x < H_c^* \sqrt{1-\alpha}$.

Now theoretically the following behaviour of the resonance fields has to be expected at a constant value of H_{px}: $H_a^* < H_{px} < H_b^*$. At $T = 0$ resonance occurs at two fields: H_c and $\sqrt{H_{px}^2 + H_c^2}$. When the temperature increases these fields become: H_c^* and $\sqrt{H_{px}^2 + \alpha H_c^{*2}}$.

At a temperature where $\sqrt{\alpha}H_b^* = H_{px}$ one has to expect also absorption in zero magnetic field. At higher temperatures this resonance field should approach the resonance field at H_c^* till at a certain temperature they melt together (at 4.2°K at $H_{px} = 11130$ Φ). At a still higher temperature only the line $H = \sqrt{H_{px}^2 + \alpha H_c^{*2}}$ remains. This is in accordance with fig. 3a of chapter I. The H_c^* curve as a function of temperature is also in rather good agreement with the curve observed by Poulis and Hardeman in proton resonance [12] and in electron resonance at very low frequencies [8].

The upper resonance field $H = \sqrt{H_{px}^2 + \alpha H_c^{*2}}$ gives the possibility to determine αH_c^{*2} as a function of temperature, see later.

The resonance field along the a-axis for $H < H_c^*$ follows Yosida 's formula (14) [6]:

$$0 = \alpha^2 H^4 - H^2\{(1+\alpha^2)\,H_{px}^2 + \alpha^2(H_b^{*2} + H_c^{*2})\} + (\alpha H_b^{*2} - H_{px}^2)(\alpha H_c^{*2} - H_{px}^2).$$

If one inserts into this formula: $H_c = 6500$ Φ; $H_b = 11300$ Φ; $H_{px} = 11130$ Φ, this formula fits well with the experimental points. It predicts resonance in zero field at 1.5°K and at a field H_c^* at 4.2°K.

I should like to make a final remark in order to review once more what happens along the a-axis when in fig. 1 the temperature is increased.

The curve $H = \sqrt{H_{px}^2 + \alpha H_c^{*2}}$ moves to the left when the temperature is increased. At $H_{px} = H_c^* \sqrt{1 - \alpha}$ a vertical line going downwards till $H_{px} = 0$ represents the orientation resonance in fig. 1 for finite temperature. When the temperature is increased, this value of H_{px} will increase too. The vertical line expands in upwards direction. At a certain temperature it will meet with the horizontal line $H_{px} = H_a^* \sqrt{\alpha}$. This happens when $H_c^* \sqrt{1 - \alpha} = H_a^* \sqrt{\alpha}$, which is at 3.7°K. At this temperature the two kinds of orientation resonances have met. The two orientation resonances link together the two curves for $H < H_c^*$ with the two curves for $H > H_c^*$, but at 3.7°K the pairs that are linked are interchanging (fig.6).

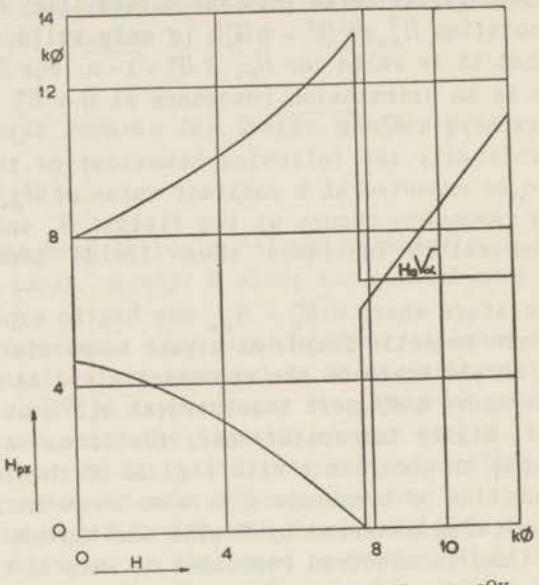

Fig. 6a. H along a-axis and $T = 3.6^{\circ}K$.

b-axis. Here the horizontal line will be $H_b^* \sqrt{\alpha}$. It will pass the frequency of measuring when $H_b^* \sqrt{\alpha} = H_{px}$. This must manifest itself by a reversal of hyperboloid curves into ellipsoid curves. It was found experimentally at 2.70°K when $H_{tracer} = 11280$ Φ. With $H_{px}^2 = \alpha H_b^{*2}$ and assuming $\alpha H_b^{*2}/H_b^{fl} = \alpha H_c^{*2}/H_c^2 = 0.84$ (at 2.70°K) one obtains: $H_b = 11270$ Φ.

This leads to: $H_a = 9200$ Φ.

c-axis. The resonance condition is:

$$\left(\frac{g_c}{g_a}\right)^2 H_z^2 + \alpha H_b^{*2} = H_{px}^2 .$$

Only at 3.55°K this resonance has been measured accurately giving $H_z = 6950$ Φ at a frequency $H_{tracer} = 11980$ Φ. This gives $H_a = 9200$ Φ.

C. *Coordinate planes*

ac-plane. Nagamiya has shown [7] that the Gorter and Haantjes hyperbola at finite temperature becomes:

$$\frac{H_x^2}{H_c^{*2}} - \left(\frac{g_c}{g_a}\right)^2 \frac{H_z^2}{H_a^{*2}} = 1 \ .$$

H_a^*/H_c^* was calculated at different temperatures in order to see if this value is independent of temperature as is supposed by Nagamiya. Most weight in determining this quantity was given to angles with the *a*-axis between 12^o and 20^o. That is done because for small angles H_a^* is very sensitive to an incertainty in H,

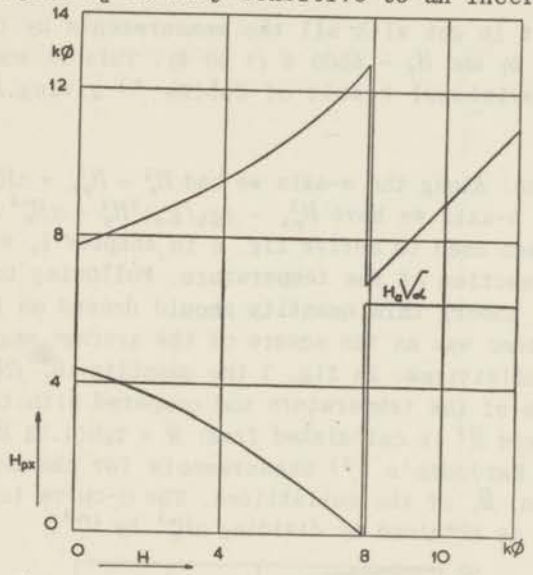

Fig. 6b. H along *a*-axis and $T = 3.8^oK$.

while big angles are much influenced by a misalignment of the crystal, as can be seen by looking at the *ab*-resonance diagrams. This admixture would give rise to a curve in the *ac*-plane lying above the threshold hyperbola.

The best fit with the experimental curves at different temperatures was obtained with $H_a^*/H_c^* = 1.4$. This gives: $H_a = 9100$ Φ.

The ellipses in the *ac*-plane obey the formula:

$$\frac{H_x^2}{\alpha H_c^{*2} + H_{px}^2} + \left(\frac{g_c}{g_a}\right)^2 \frac{H_z^2}{H_{px}^2 - \alpha H_a^{*2}} = 1 \ .$$

These ellipses gave the best fit with the experiments of curve II fig. 8a with $H_a(0^o) = 9500$ Φ. Curve I gave: $H_a = 9200$ Φ.

4. **Summary of these determinations**

H_a	Experiment
9100 Φ	Threshold hyperbola
9500 and 9200 Φ	*ac*-ellipses
9200	Reversal of *b*-axis curves
9200	Low line; *a*-axis
9200	Resonance along *c*-axis
9100	*ab*-plane; *a*-curve
9100	*ab*-plane; *b*-curve

A good fit is got with all the measurements by taking: H_a = 9150 Φ (± 50 Φ) and H_c = 6500 Φ (± 50 Φ). This is somewhat lower than the provisional result of Ubbink [4] giving H_a = 9700 Φ (± 500 Φ).

αH_c^{*2} values. Along the *a*-axis we had $H_x^2 - H_{px}^2 = \alpha H_c^{*2}$.

Along the *b*-axis we have $H_{px}^2 - (g_b/g_a)^2 H_y^2 = \alpha H_c^{*2}$. These formulae have been used to derive fig. 6 in chapter I, where αH_c^{*2} is given as a function of the temperature. Following to Nagamiya's and Yosida's theory this quantity should depend on the temperature in the same way as the square of the average magnetic moment of the two sublattices. In fig. 7 the quantity $\alpha H_c^{*2}/H_c^2$ is plotted as a function of the temperature and compared with the theoretical curve where $\bar{M}^2$ is calculated from: $\bar{M} = \mathrm{tgh}(4.33\ \bar{M}/T)$ and with Poulis' and Hardeman's [12] measurements for the square of the magnetization, $\bar{M}$, of the sublattices. The α-curve in the experimental paper is obtained by dividing αH_c^{*2} by H_c^{*2}.

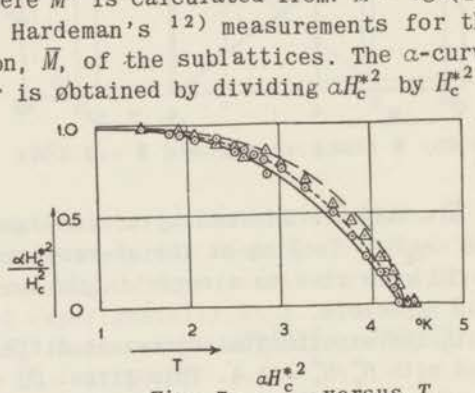

Fig. 7. $\frac{\alpha H_c^{*2}}{H_c^2}$ versus T.

– – – – – curve of $\bar{M}^2$ by proton resonance [12]
– · – · – curve of $\alpha H_c^{*2}/H_c^2$ from susceptibility measurements [14]
——— $\bar{M}^2$ with molecular field theory

Both gave nearly the same result but the curve obtained from the *b*-axis experiments deviated appreciably from the *a*-axis curve near the Néel temperature. This can be ascribed to the fact that Yosida's assumptions are no longer valid. It has been found by

Poulis and Hardeman [13] that the Néel temperature is lowered by a magnetic field, especially along the a-axis. That is in accordance with the different Néel temperatures in our measurements for a- and b-axis. The scattering of the points is due to the difficulty to determine the magnetic resonance fields accurately enough, while aH_c^{*2} is a small quantity with respect to H^2 and H_{px}^2. It is also not quite certain if one may use the same g-values as were obtained by the paramagnetic resonance.

Chapter III

SOME FURTHER DETAILS OF THE ANTIFERROMAGNETIC RESONANCE DIAGRAM AT 9500 MHz

1. Introduction

A number of papers have shown that there is good general agreement between the molecular field description of the antiferromagnetic resonance diagrams and experiment [1)3)]. Two discrepancies have been observed, however, in the course of careful remeasurements. These are actually rather sensitive tests of the theory, which is perhaps in too simplified a form at present in spite of its already complicated nature.

The experimental method will be described in chapter IV, section 2.

2. The resonance diagram in the *ab*-plane

The first point concerns the shape of the $H_{res.}$ vs β curve in an *ab*-crystal at the lowest temperatures, at 1.4°K, and at 9500 MHz. The equations of Yosida and Nagamiya are used since they take into account the effects of finite temperature [7)]. The resonance diagram is expressed by two equations in the unknowns ψ and H, where H is the magnitude of the static external resonance field and ψ is the angle which the spins take up with respect to it in the static case. These are equations (3.9) and (4.1) of reference [7)], which are reproduced here with the g-values written in explicitly and the anisotropy fields expressed in the notation of Ubbink (the * means $T \neq 0$).

$$0 = e^2 - e\,[\eta(\alpha^2\cos^2\psi + 1) + \rho\cdot + \cos^2(\psi-\beta) - 2\sin^2(\psi-\beta)$$

$$- \eta\,[\alpha\cos^2\psi\cos 2(\psi-\beta) + \alpha\sin\beta\cos\psi\sin(\psi-\beta)$$

$$+ \cos\beta\sin\psi\sin(\psi-\beta) + \rho\cdot(\alpha\cos^2\psi - \sin^2\psi)]$$

$$+ \eta^2\alpha^2\cos^2\psi + [\rho - \sin^2(\psi-\beta)]\cos 2(\psi-\beta) \qquad (1)$$

and

$$\sin 2(\psi-\beta) = \alpha\,\eta\sin 2\psi \qquad (2)$$

where $\eta = \frac{1}{\alpha}\left(\frac{2}{g_a}\frac{H'}{H_c^*}\right)^2$, $e = \frac{H_{px}^2}{\alpha H_c^{*2}}$, $\rho = \frac{H_b^{*2}}{H_c^{*2}}$,

$$\alpha = 1 - \frac{\chi_{\parallel}}{\chi_{\perp}}, \qquad H_{px} = \frac{\omega}{\gamma_a}$$

and $$H'^2 = \left(\frac{g_a}{2} H_x\right)^2 + \left(\frac{g_b}{2} H_y\right)^2 = \left(H_{exp}\frac{g\beta}{2}\right)^2$$

with $H_x = H_{exp}\cos\beta$ and $H_y = H_{exp}\sin\beta$

Equation (2), usually written $\operatorname{tgn} 2\psi = \frac{\sin 2\beta}{\cos 2\beta - \alpha\eta}$, was originally derived by Néel.

The mist convenient way to solve these seemed to be to eliminate H and first solve, by numerical iteration, for β as a function of $(\psi-\beta)$. This function is of some interest in itself and is shown in fig. 1, together with points obtained from equation (2) and the experimental values of H which are shown in fig. 2.

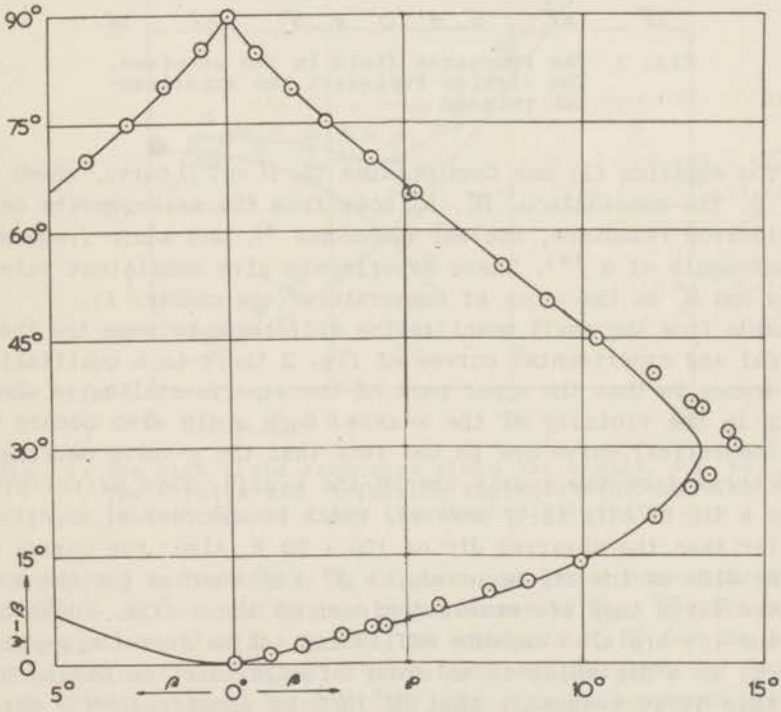

Fig. 1. Angle between the direction of the spins and the a-axis, $\psi-\beta$, as a function of β. The drawn curve is the theoretical curve, and the circles are obtained by applying the formula of Neel, formula 2, on the experimental points of fig. 2.

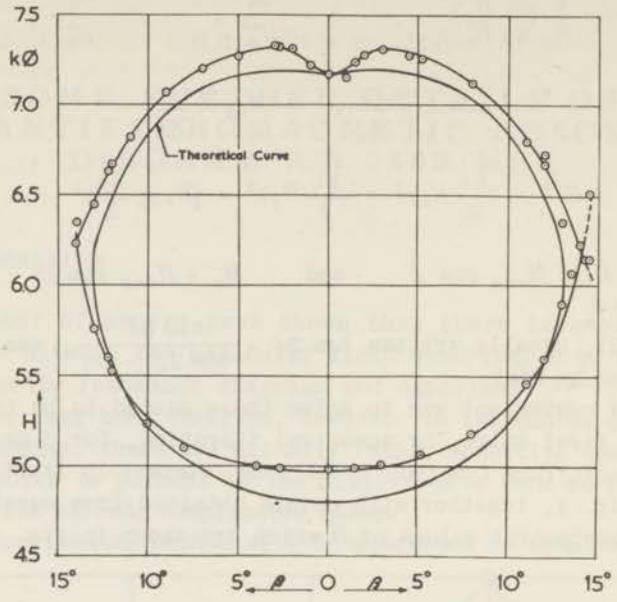

Fig. 2. The resonance field in the ab-plane. The circles represent the experimental values.

From equation (2) one then obtains the H vs. β curve, shown in fig. 2. The constants α, H_c^*, H_b^* come from the measurements on 8 mm electron resonance, nuclear resonance [8], and audio frequency measurements of α [14]. These experiments give consistent values for α and H_c^* as functions of temperature (see chapter I).

Aside from the small quantitative difference between the theoretical and experimental curves of fig. 2 there is a qualitative difference in that the upper part of the experimental curve shows a dip in the vicinity of the a-axis. Such a dip also occurs in the theoretical curve due to the fact that the g-value decreases as H turns from the a-axis toward the b-axis. This effect produces a dip of only 15 Φ, however, which is an order of magnitude smaller than the observed dip of 120 ± 20 Φ. Also, the maxima on either side of the dip occur at $\beta = 3^o \pm \frac{1}{2}^o$ whereas for the calculated curve they are somewhat closer to the a-axis. Equations (1) and (2) are also capable of leading, aside from the g-value effect, to a dip which is an order of magnitude too small, but for this it is necessary that H_b^{*2}/H_c^{*2} be greater than 3 while according to the best data it is 2.98. This last effect would rapidly disappear with rising temperature, whereas the magnitude of the observed dip is essentially unchanged up to 3.5°K.

3. Variation of H_H with temperature

Fig. 3 shows the position of the higher resonance along the a-axis, H_H, as a function of temperature. As can be seen from the results of the previous section, measurements with ac-crystals can easily be ambiguous due to slight misorientations of the field toward the b-axis. In most cases, therefore, the results are taken from the minimum in the dip observed in ab-crystals, and the lower values have been favored in drawing the experimental curve.

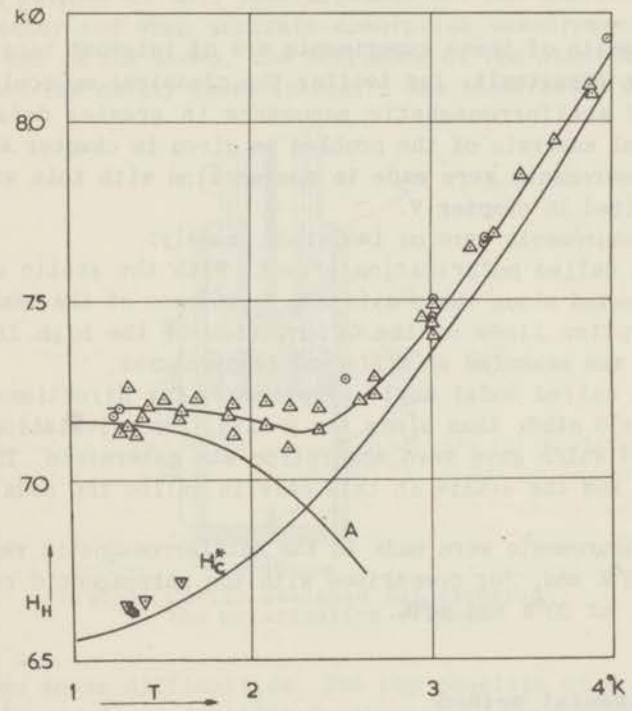

Fig. 3. The high field resonance along the a-axis, H_H, vs. T. The circles and triangles represent the experimental values; H_c^* and A are the theoretical curves.

According to the theory H_H is given, at lower temperatures, by $H_H^2 = H_{px}^2 + \alpha H_c^{*2}$ and at higher temperatures by $H_H = H_c^*$. The cross over point occurs at $T = 2.3^oK$. The constants α, H_c^* for the lower or theoretical line in fig. 3 have been obtained from the experiments [8)14)] mentioned in chapter I. The 3 cm measurements are not quite consistent with these other experiments and with the theory since the 3 cm H_H values lie from 100 to 200 Φ too high.

Chapter IV

MEASUREMENTS ON THE INTENSITY OF THE RESONANCE ABSORPTION AT FREQUENCIES BETWEEN 9300 AND 9500 MHz

1. Introduction

The results of these experiments are of interest because they provide an opportunity for testing the classical molecular field theory of antiferromagnetic resonance in greater detail. The theoretical analysis of the problem is given in chapter VI. Linewidth measurements were made in conjunction with this study and are described in chapter V.

The measurements were of two kinds, namely:

a. The so called polarization effect. With the static external field oriented along the a-axis the dependence of the peak of the two absorption lines on the orientation of the high frequency field, **h**, was measufed at different temperatures.

b. The so called nodal angle experiment. For directions of the static field other than along the a-axis, the orientation of the h.f. field which gave zero absorption was determined. The angle between **h** and the a-axis in this case is called the nodal angle, η.

The measurements were made in the antiferromagnetic range from 1.2 to 4.3°K and, for comparison with the paramagnetic resonance intensity, at 20°K and 80°K.

2. Experimental method

A. *Apparatus*

The previous 3 cm measurements were carried out in a cylindrical cavity used in transmission. The construction of this cavity is given by J.Ubbink in his thesis. The crystals were placed in the center at the bottom of the cavity, which was excited in the TE_{111} mode, so that the h.f. field, static field and a-axis were all lying in the horizontal plane. It was not possible during a particular experiment to vary the angle between the crystal axes and the h.f. field. In addition to this shortcoming it also occurred that two modes of oscillation existed in this cavity. The difference in the resonance frequencies of these two modes was 12 MHz and the magnetic field lines of one mode were

perpendicular to those of the other, as could be determined by rotating the static field and measuring the positions where the intensity of the paramagnetic resonance line was minimal for both modes.

The origin of the existence of the two modes must be sought in a small deviation of the cavity from cylindrical symmetry, as was already remarked by Ubbink, and is most likely due to the presence of the coupling loops. In a perfect cylindrical cavity the direction of the h.f. magnetic field in space is undetermined.

For the purpose of this investigation the two modes were too close together and when accurate absorption measurements were done with one of the modes, the influence of the other mode was troublesome. The cavity shown in fig. 1 was constructed in order

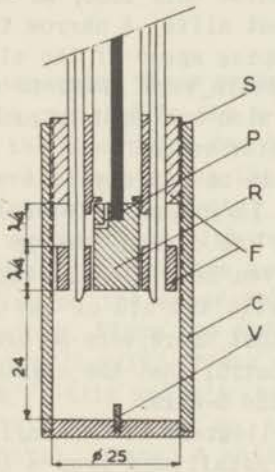

Fig. 1. Cavity designed for studying the polarization effect.

to overcome these difficulties. The top consists of a central cylinder (R) which can be rotated externally, surrounded by the fixed annular cylinder (F) through which the coupling loops pass. The remainder of the cavity is a can (C) which screws on to the top by a fine thread (S). A 2 mm high vane (V) which is soldered along a diameter in the buttom of the can produces the required separation of the two modes of oscillation, one of which is such that the E-lines are perpendicular to the vane and the other such that they are parallel to the vane.

A simple way of considering the resulting difference in frequency between the modes, suggested by B.Bolger, is to consider that since E-lines cannot be parallel to the vane at the bottom, the cavity length is effectively 1 or 2 mm greater for the mode in which E-lines are perpendicular to the vane.

The screw thread (S) made it easy to open the cavity and to tune it to the klystron frequency. Although the cavity was tuned at room temperature, the increase of resonant frequency at helium temperature was only 50 MHz, which was well within the possible tuning range of the klystron. Greasing the thread with silicone grease made the cavity tight against helium I which would otherwise produce too much noise due to bubbling. Helium II leakage was tolerable since there is no bubbling in it.

The helium II leakage, incidentally, was observed as a slow drift in the resonant frequency of the cavity, which suggested a possibility for measuring flow rates.

$\lambda/4$ traps were constructed in F in order to reduce electrical losses in the annular slits between F and C and between R and C. The Q-factor was nevertheless only 2000, as compared to values of 10000 for cavities without slits. A narrow tube (P) was drilled in R to increase the pumping speed of the slit between R and F. The copper chloride crystals were glued to the rotatable table with Duco cement, which also was used to protect their surfaces from disintegration by water vapor.

Measurements were made on six crystals weighing between 10 and 20 mg. This size was large enough for sufficient sensitivity and small enough so that the crystal was in a region of uniform h.f. field. The data given here are all reduced to 10 mg. The crystals were examined with the aid of the polarization microscope in order to check that there were no cracks or disintegrated regions and also to control that the crystal was well cut perpendicular to the *c*- or the *b*-axis.

A crystal of a few milligrams of diphenyl trinitrophenyl hydrazine free radical crystallized from a benzol solution was cemented together with the copper chloride. The free radical was used for several different purposes.

One of its functions was the following: The intensity of the paramagnetic line of the free radical is proportional to $\sin^2\zeta$, where ζ is the angle between static and h.f. field, so that the direction of the h.f. field in space can be determined very precisely (within one degree) from the position where the absorption is minimum. The minimum was usually less than 0.3% of the maximum, which is a measure of the uniformity of the h.f. field over the area of the free radical crystal.

The free radical absorption intensity also served as a check on the change of the Q-factor when rotating the table. Finally it served as a reference for relating the paramagnetic and antiferro magnetic absorption of copper chloride.

The transmitted microwave signal was detected by a 1N21 diode and was observed either with a sensitive galvanometer or by oscilloscope display with the aid of a 50 Hz sweep field. The

latter was convenient for part b: the nodal angle experiment. For the polarization effect, measurements were done only with the galvanometer, since it enables one to avoid errors due to the dispersion of the cavity by retuning the klystron at each point. The relative absorption was computed with the expression: $(\sqrt{\delta_o/\delta} - 1)$, where δ_o is the galvanometer deflection far off resonance and δ is the deflection at some point in the line. This expression is proportional to the absorption coefficient if the diode may be assumed to be a square law rectifier, a point which was checked independently by means of a callibrated attenuator and also from time to time during the measurements by observing that the free radical absorption intensity followed very closely the $\sin^2\zeta$ law (see section 4).

B. *Procedure*

a. Polarization measurements. These measurements were carried out with the static field parallel to the *a*-axis. We were interested in the intensity of the absorption for different orientations of the h.f. field, **h**, with respect to the *a*-axis. Since the h.f. field was fixed in space, the crystal was rotated so that the *a*-axis assumed a given position with respect to **h** and then the static field **H** was aligned along the *a*-axis by turning the magnet, and by observing on the scope where the lower resonance field, H_L, was a minimum. Since the absorption intensity of the low line was zero for **h**//*a*-axis, it was of more interest to study the absorption for **h**//*b*-axis and **h**//*c*-axis. It was unfortunately not possible to do this in our set up, because **h** and **H** were both in the same, horizontal, plane. A solenoid magnet providing a vertical magnetic field of about 5000 Φ and big enough to contain the cryostat was not available.

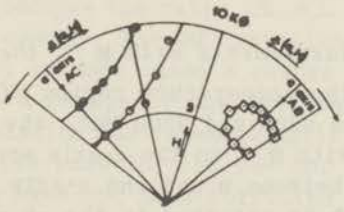

Fig. 2. Resonance diagrams obtained with an *ab*- and an *ac*-crystal mounted together in the cavity.

However, by mounting an *ab*- and an *ac*-crystal with their *a*-axes at right angles the resonance diagrams of the two crystals do not intersect (fig. 2) and it was possible to make measurements on both crystals in the same run. It was found with the aid of the free radical absorption that the intensity of the h.f. magnetic

field varied only a few per cent over the area of the table so that the exact positions of the crystals on the rotatable table with respect to the coupling loops were not critical.
b. Nodal angle measurement. Nodal angles were measured in an *ab*-crystal at 1.4°K. By rotating the crystal, various fixed angles between the *a*-axis and the h.f. field were established. For each position the external field was rotated and simultaneously its magnitude was changed so as to remain on top of resonance. The resonance line was thus kept on the scope and its intensity was found to vanish for a certain angle β between the external field and the *a*-axis. This angle β depended upon the fixed angle η between the h.f. field and the *a*-axis, and was studied for both low and high line.

After the determination of the orientation of the magnet which gave a vanishing absorption intensity, the magnet was rotated and simultaneously the magnitude was decreased so that one could follow the low line until the magnet was parallel with the *a*-axis indicated by the fact that the fieldstrength was a minimum. This reading gave the orientation of the *a*-axis. Then the fieldstrength was reduced till the free radical line appeared on the scope. Again the magnet was rotated until the intensity of the free radical line disappeared, indicating the fact that now **H** was parallel with **h**. The precision of the three orientations is of the order of ½°.

The alternative of turning the crystal for a fixed angle between **H** and the *a*-axis was less accurate, since turning the crystal produced much noise on the scope signal, due to vibrations in the cavity.

3. Results

A. *Polarization measurements with* **H** // *the a-axis*

a. $\sin^2\zeta$ law. In the temperature region of 1.3 – 1.4°K and at frequencies between 9300 and 9500 MHz, the intensities of the low and high line with **H** // to the *a*-axis were studied as a function of the angle between **h** and the *a*-axis. This angle will be called ζ (b) when **h** is situated in the *ab*-plane and ζ (c) when **h** is situated in the *ac*-plane.

It was found experimentally that the intensities of both low and high line were zero when **h** was parallel to the *a*-axis; that they had a maximum in the *ab*-plane when **h** // *b*-axis and in the *ac*-plane when **h** // *c*-axis.

In both planes it was found that the intensity was proportional to $\sin^2\zeta$.

In the discussion that follows the symbols which will be used are:

ACL: Peak intensity for **H**//a-axis; **h**//c-axis; Low line ($H < H_c^*$)
ABL: " " " **H**//a-axis; **h**//b-axis; Low line
ACH: " " " **H**//a-axis; **h**//c-axis; High line ($H > H_c^*$)
ABH: " " " **H**//a-axis; **h**//b-axis; High line

The results of $\sin^2\zeta$ measurements at 1.35°K were:
ABL/ACL = 1.45 (± 0.1). ABL/ABH = 8 (± 2). ABH/ACH = 4 (± 1).

b. ABL/ACL versus temperature. The results of four different runs is compiled in fig. 3. The drawn curve is the theoretical

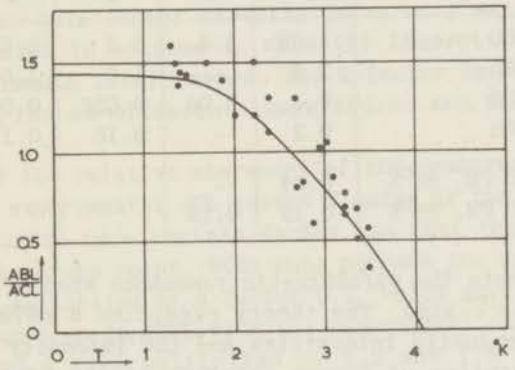

Fig. 3. Polarization effect for the low-line. Experimental points and theoretical curve (chapter VI).

curve and will be explained in chapter VI. Although it is a dubious procedure to compare different runs with each other, due to the different Q-factor for each of the runs, this difficulty did not show up here, because the ratio ABL/ACL was obtained from each run in the same cavity. The 90° rotation from ab-crystal to ac-crystal produced in some cases a change in the Q-factor, manifesting itself in a change of the free radical absorption intensity. Then the rotation was repeated until the free radical absorption was about the same for the ab- and the ac- orientation. The experiments have not been corrected for this effect, because the difference in the free radical absorption was usually less than 10% and only available for a small number of ABL and ACL values.

c. ACL versus temperature. In order to obtain a sufficient number of experimental points, four different runs were compared with each other, each run including absorption values at different temperatures. Measurements at 80°, 20°, 4°K and 1.3°K showed no dependence of the Q-factor on the temperature, but in the course

of the experiments a lowering of the Q-factor was observed from one run to the next. This is most likely due to the gradual disappearance of the silver coating of the rotatable table on which the crystals were glued, and to the fact that in the last run bigger crystals were used, with a relative increase of dielectric losses in the cavity. The readings were:

Intensities of the peak absorption in the temperature range of 1.3 - 1.4°K and frequencies between 9300 and 9500 MHz, all calculated for 10 mg material.

Line	run 1	2	3	4
ACL	1.65	1.4	1.1	0.62
ABL	2.5	-	1.6	1.0
ACH	0.1	0.06	0.032	0.04
ABH	0.3	-	0.18	0.17
AC PM. 80°K	0.04	-		
AC PM. 20°K	0.15	0.19		

AC PM. represents the paramagnetic resonance when **H** // a-axis and **h** parallel the c-axis. The theory predicted a relation between the antiferromagnetic intensities and the intensity of the paramagnetic absorption of copper chloride at the Néel temperature 4.3°K. In order to obtain this intensity at 4.3°K, two methods were used, leading to the same result.

The most straight forward method is to use the theoretical prediction, that the intensity of the paramagnetic resonance absorption is proportional to the susceptibility, and thus inversely proportional to $(T - \theta)$. Using the experimental values of the absorption for copper chloride at 80° or 20°K, the paramagnetic resonance intensity at 4.3°K has been obtained by extrapolation, taking θ equal to -5° (ref.11). No physical conclusions will be drawn from this hypothetical quantity, because the paramagnetic linewidth at 4.3°K is not known, but its usefulness will appear later in the theoretical discussion (chapter VI).

Another method was to measure the intensity of the free radical together with the intensity of the copper chloride at a temperature where the copper chloride is paramagnetic. Normalizing to 10 mg free radical, it was found that the intensity of the free radical was 4 times that of 10 mg copper chloride at 80° and 20°K. At helium temperature the free radical remained paramagnetic and one would expect the intensity of the copperchloride at 4.3°K to be $\frac{1}{4}(4.3 + 0.1)/(4.3 + 5)$ times the intensity of the free radical at that temperature. The θ of the free radical has been measured to be 0.1° (ref.9). It was checked in the first two runs that the

results of both methods were the same and in the fourth run the AC PM. 4.3 K is obtained only from the free radical reading.

It may be remarked that at temperatures below $4^{o}K$, the free radical peak intensity increased much more slowly than $1/T$ for decreasing temperature and at the same time the linewidth increased. This made the substance less applicable for intensity meter than was at first thought.

The experimental values obtained for the intensities of the peak absorption are only relative to each other. The constant that would transform these values into absolute numbers is proportional to the Q-factor of the cavity and to a factor, which depends upon the magnetic field-distribution in the cavity. One cannot measure this factor directly in an easy way, but a rough estimate is made in section 4, when the theoretical background of the experiments is discussed. The Q-factor was only measured in the first run at different temperatures and was found to be 2000.

Because of the relative character of the measurements, one can multiply the experimental ACL versus T curve or the corresponding theoretical curve by a certain factor, so that the curves coincide at least in one point. With this purpose the readings of run 1 and 2 were multiplied by a factor 0.7, which gave a nice fit at all temperatures up to $80^{o}K$ with the theoretical curve. The readings of 3 and 4 were multiplied by 1.2 and 1.5 respectively, which is supposed to give the intensity values if the Q-factors would have been as high as 2000. In this way a good mutual agreement is obtained between the four runs at all temperatures.

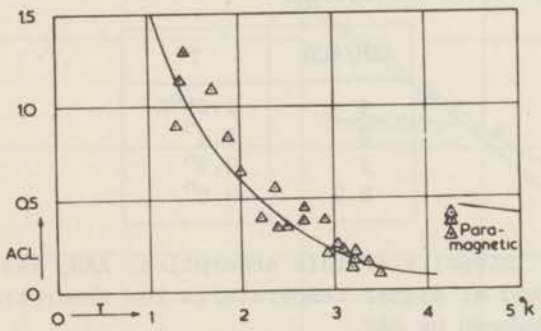

Fig. 4. Intensity of the peak of the resonance line ACL versus temperature. The experimental points are obtained in different runs.

In fig. 4 the measurements of the ACL intensities at different temperatures are collected, together with the extrapolated paramagnetic intensities. The drawn curve is the theoretical curve, to be explained in the next chapter.

d. Peak-intensities at 1.35°K, compared with the theoretical values. When using the factors of multiplication of the foregoing section on the data compiled in the table, one gets:

Line	run 1	2	3	4	Theory
ACL	1.15	1.0	1.3	0.9	1.10
ABL	1.75	–	1.9	1.5	1.57
ACH	0.07	0.04	0.04	0.06	0.065
ABH	0.21	–	0.22	0.25	0.30
AC PM. 80°K	0.03				0.05
AC PM. 20°K	0.10	0.13			0.16
AC PM. 4.3°K (extrapolated)	(0.3)	(0.4)		(0.4)	0.45
Free radic. 80°K	0.10				
Free radic. 20°K	0.40				
Free radic. 4.3°K	2.0			3.0	

e. High line intensity. Some measurements were done on ABH/ACH versus temperature. The high line intensity and the linewidth are very sensitive to small errors in the alignment of **H** along the a-axis, which must be one of the reasons for the scattering of this value at 1.35°K.

It may be remarked that above 2.3°K the resonance is the so called orientation resonance (see page 22). Above that temperature it was found experimentally that a h.f. field along the a-axis also produced absorption.

ABH/ACH	T
4	1.35°K
2	2.4°
1	2.7°
0.3	3.0°

At 3.0°K the intensity of this absorption, AAH, was even about 2 times ACH and at higher temperatures the absorption was predominantly produced by AAH.

f. Nodal angle experiment. This experiment was done in an ab-crystal at 1.4°K and 9520 MHz. As was already remarked, the nodal angle η equals zero when β equals zero for both high-line and low-line. For values of β different from zero, the high- and low-line behaviour was different, not only quantitatively but also qualitatively. This will be demonstrated for the case: $\beta = 5^{\circ}$.

Position of the a-axis, **H** and **h** for zero absorption intensity of high- and low-line; $\beta = 5^{\circ}$.

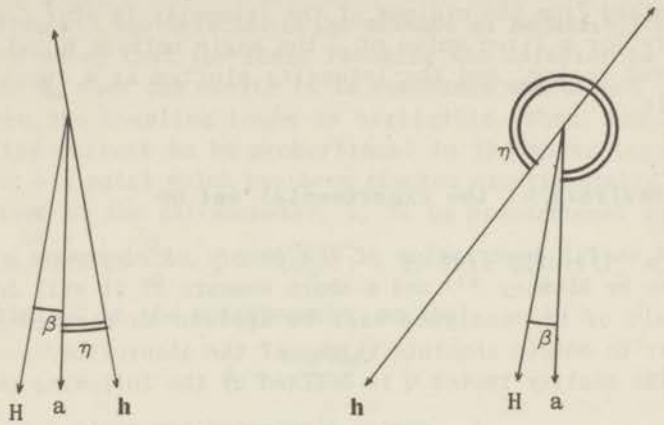

Low line High line

We therefore denoted the nodal angle, η, for the low-line as 12°, but for the high-line as 180°-50°.

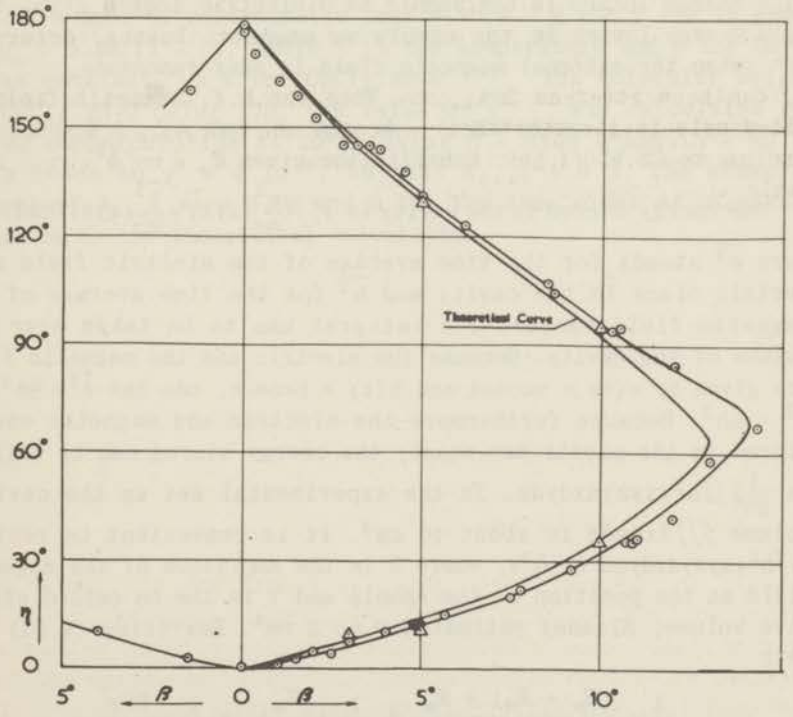

Fig. 5. Nodal angles in the ab-plane at 1.4°K, together with the theoretical curve.

The results of the measurements are given in fig. 5, together with the theoretical curve. The points at $\beta = 0^o$, 5^o and 10^o were obtained from the minimum of the intensity in $\sin^2 \zeta$ measurements where for a fixed value of β the angle between **h** and the a-axis, ζ, was varied, and the intensity plotted as a function of that angle.

4. Analysis of the experimental set up

A useful description of the theory of microwave resonance is given by Bleaney [21] and a short summary of it will follow. The result of the analysis will be applied to the measurements in order to obtain absolute values of the absorption.

The quality factor Q is defined by the following relation

$$\frac{1}{Q} = \frac{\text{energy dissipated per cycle}}{2\pi(\text{energy stored in cavity})} \qquad (4.01)$$

The energy dissipated per cycle can be written as $E_w + E_d + E_m$ where the meaning of the symbols is

E_w = Energy losses in the wall of the cavity.

E_d = Energy losses in the sample as dielectric losses.

E_m = Energy losses in the sample as magnetic losses, occurring when the external magnetic field is near resonance.

E_m can be written as $2\pi A_{sec}/\omega$. When the h.f. magnetic field in the sample is given by $\delta\mathbf{H}(t) = \mathbf{h}\cos\omega t$ one has $A_{sec} = \frac{1}{2}\omega\chi'' h^2$, according to Ch.VI (1.11). Substitution gives $E_m = \pi\chi'' h^2$.

The energy stored in the cavity is $\iiint\{\frac{\overline{e^2}}{8\pi}(xyz) + \frac{\overline{h^2}}{8\pi}(xyz)\}dxdydz$.

Here $\overline{e^2}$ stands for the time average of the electric field at a certain place in the cavity and $\overline{h^2}$ for the time average of the magnetic field vector. The integral has to be taken over the volume of the cavity. Because the electric and the magnetic field are given by $e(t) = e\cos\omega t$ and $h(t) = h\cos\omega t$, one has $\overline{e^2} = \frac{1}{2}e^2$ and $\overline{h^2} = \frac{1}{2}h^2$. Because furthermore the electric and magnetic energy stored in the cavity are equal, the energy stored can be written as $\frac{1}{8\pi}\iiint h^2(xyz)dxdydz$. In the experimental set up the cavity volume $\iiint dxdydz$ is about 10 cm^3. It is convenient to replace $\iiint h^2(xyz)dxdydz$ by h^2V, where h is the amplitude of the magnetic field at the position of the sample and V is the so called effective volume; Bleaney estimated V as 3 cm^3. Rewriting (4.01) one gets

$$\frac{1}{Q} = \frac{(E_w + E_d) + E_m}{\frac{1}{4}h^2V} \cong \frac{1}{Q_o} + \frac{E_m}{\frac{1}{4}h^2V} = \frac{1}{Q_o} + \frac{4\pi\chi''}{V}$$

so that $$\frac{4\pi\chi'' Q_o}{V} = \frac{Q_o}{Q} - 1$$

Here Q_o represents the Q-factor in the absence of magnetic losses.

It may be shown that the power reaching the detector is proportional to Q_o when the cavity is in resonance and direct coupling between the coupling loops is negligible. Then, assuming the rectified current to be proportional to the power input to the detector – a point which has been checked experimentally – and the deflection of the galvanometer, δ, to be proportional to the current, one obtains $\frac{Q_o}{Q} - 1 = \sqrt{(\delta_o/\delta)} - 1$. This quantity, A, was actually obtained in the measurements, so that =

$$A = \frac{4\pi\chi'' Q_o}{V} \qquad (4.02)$$

δ_o stands for the deflection far off resonance.

Q_o has been measured as 2000 and V will be taken as 3.

For the peak of the χ'' vs. H curve one can write $\chi''_{peak} = \chi_o \frac{H}{\Delta H}$, according to Ch.VI (1.10). The static susceptibility, χ_o, of a mole of paramagnetic ions with S = ½ and g = 2 is given by $\chi_o = 0.38/(T - \theta)$, where T is the temperature and θ the Curie Weiss constant, -5^oK for $CuCl_2.2H_2O$ [11]. The molecular weight of $CuCl_2.2H_2O$ being 170, the value of χ''_{peak} was calculated for 10 mg copperchloride at 20^oK taking $H = 3100$ Φ and $\Delta H = 80$ Φ. This leads to $\chi'' = 4\ 10^{-5}$, so that $A_{peak} = 0.3$. The measured values of A_{peak} were 0.15 and 0.19, the same order of magnitude as given by the theoretical calculation.

Chapter V

ANTIFERROMAGNETIC RESONANCE LINEWIDTHS AT 9400 MHz

1. Experimental

The same transmission cavity method was used as is described in chapter IV. The crystals were cemented to the rotatable central part of the top of the cavity, where they were in a region of horizontal h.f.field. Crystals with good *ab*- or *ac*-planes were selected by the aid of a polarization microscope (see page 11). By comparison with the known behaviour of the resonance diagram below the Néel point and measurement of *g*-values above, it was checked that the *c*- or *b*-axis respectively was vertical in the cavity within a few degrees.

Resonance lines were observable either by oscilloscope display or by point by point measurements with a sensitive galvanometer. The former method was used for orienting the static field and for rough linewidth determinations. The accurate linewidth data were, however, obtained by the galvanometer, since by retuning the klystron, errors due to dispersion of the cavity are eliminated. The relative values of magnetic field going across a resonance line were measured by the simple circuit of fig. 1 which made the readings easy and accurate.

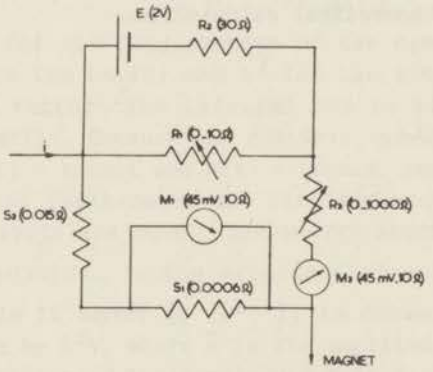

Fig. 1. Compensation circuit for measuring linewidths.

R_1 is adjusted so that meter M_2 reads null at one side of the line. R_3 is then reduced to zero for maximum sensitivity of M_2.

M_1 reads the total current and M_2 the relative current. The combination of S_2 and S_1 leads to an increased sensitivity of meter M_2 over M_1 of $(S_1 + S_2)/S_1(1 + \frac{R_1R_2}{R_M(R_1 + R_2)}) \approx 10$ in our set-up.

2. Results

Data are given from measurements on six well grown crystals.

A. *The resonance field parallel to the crystal axes*

a) The most detailed measurements were made for the case of static external field parallel to the *a*-axis. In this situation there are two resonance fields, H_L and H_H, respectively smaller and greater than the critical field, H_c^*. For temperatures above 2.3°K, H_H is very nearly equal to H_c^*. The temperature variation of H_L and H_H has been discussed already by Ubbink and a graph has been included here, fig. 2, for reference. The paramagnetic line, which exists above 4.32°K, is at 3050 Φ for the frequency of this experiment. The width between points of half intensity at liquid air temperature is 86 Φ along the *a*-axis and 70 Φ along the *b*-axis [10] and we found very nearly the same values at liquid hydrogen temperatures.

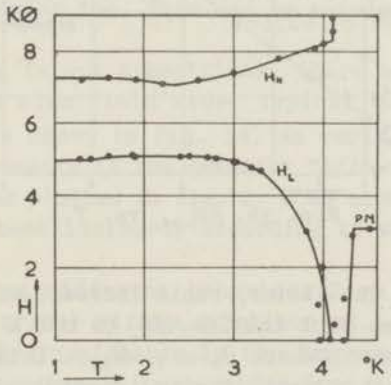

Fig. 2. Resonance fields along the *a*-axis vs. *T*.

The temperature dependence of the width at half the maximum of the H_L line, ΔH_L, will be described first, see fig. 3a. It should be noted that up to 3°K, H_L is almost independent of temperature and equal to 5 KΦ, see fig. 2. The width, ΔH_L, measured in oersteds, increases from very small values to 140 Φ at 3°K and then increases further very rapidly to about 3000 Φ at 4.1°K where H_L

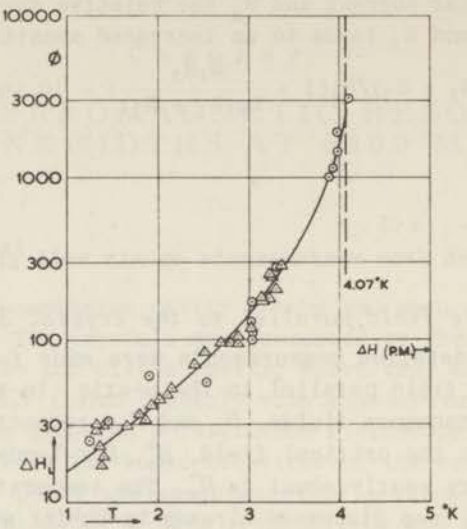

Fig. 3a. Linewidth of H_L vs. T.

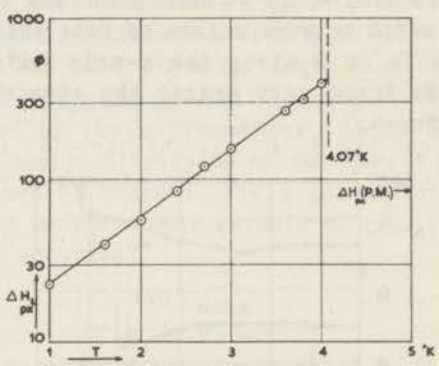

Fig. 3b. ΔH_{Lpx} vs. T.

decreases to zero. The latter, rapid increase of ΔH_L is probably associated with the fact that $d\omega/dH_L$ is not a constant as in the paramagnetic case (where $H_x=\omega/\gamma_x=H_{px}$). Thus, at 4.07°K, $H_L=0$ and $d\omega/dH_L=0$ so that a small finite linewidth in frequency, $\Delta\omega$, produces a very wide line in magnetic field, ΔH. It is not sure as to whether the mechanism of line broadening is a magnetic type interaction, which must be described by a ΔH, or a lifetime reducing type interaction, which produces a $\Delta\omega$.

To see the effect of the temperature dependence of $d\omega/dH$, the quantity $(dH_{Lpx}/dH_L)_{Av}$ was calculated, where H_{px} represents the frequency expressed as the paramagnetic resonance field, and the average is carried out over ΔH_L. This is illustrated in fig. 4a for T = 3.6°K and 2.2°K and fig. 4b is a graph of $(dH_{Lpx}/dH_L)_{Av}$

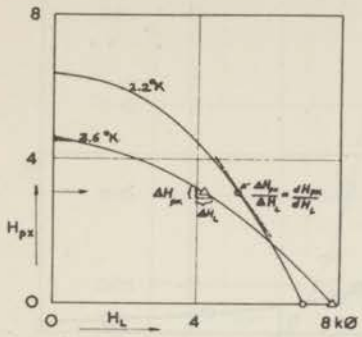

Fig. 4a. Part of the a-axis resonance diagram at 2.2 and 3.6°K.

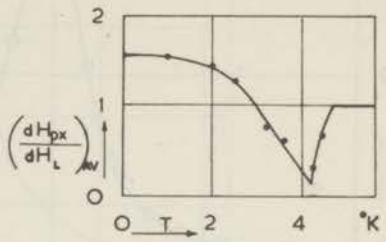

Fig. 4b. $\left(\frac{dH_{Lpx}}{dH_L}\right)_{Av}$ vs. T at 9400 MHz.

vs. T. It was then possible to plot the linewidth in frequency, i.e. ΔH_{Lpx}, which is shown in fig. 3b. When plotting the data on semi-logarithmic paper it was found that ΔH_{Lpx} can be expressed very closely by the empirical relation $\Delta H_{Lpx} = 9 \exp (T/1.05^{\circ}K)$ Φ.

As will be shown in Ch. VI, the oscillation of the net magnetization vector is circular when $\omega/\gamma_x = \alpha H_x$, which occurs at 2.9°K. At this temperature $\Delta H_L = \Delta H_{px} = 120$ Φ, a value which is of the same order of magnitude as in the paramagnetic region where the precession is circular too. This may be purely accidental, however.

The shape of H_L is not symmetrical, there being a characteristic tail on the high field side. Typical galvanometer plots of this effect are shown in fig. 5a. An empirical quantitative measure of the asymmetry is the quantity "h/l" defined in fig.5a. This ratio has been plotted in fig. 6. Some unpublished data from Ubbink have also been included, according to which h/l is somewhat smaller.

H_H showed a very different behaviour from H_L, being in the first place symmetrical within experimental accuracy, fig. 5b. Two regions are distinguishable in the temperature variation of ΔH_H, fig. 7. Going down in temperature from 2.5 K to the lowest temperature accessible to us, 1.24°K, the linewidth increases very rapidly.

From 2.5 to 3.4°K the linewidth is approximately constant and narrower than for the paramagnetic line, viz., $10\ \Phi < \Delta H_H < 30\ \Phi$. Above 3.4°K it increases slowly again. The large amount of scatter in the points of ΔH_H vs. T is due primarily to the strong dependence of ΔH_H on the angle β between H_H and the a-axis, as will be described below in B. The graph was drawn taking into

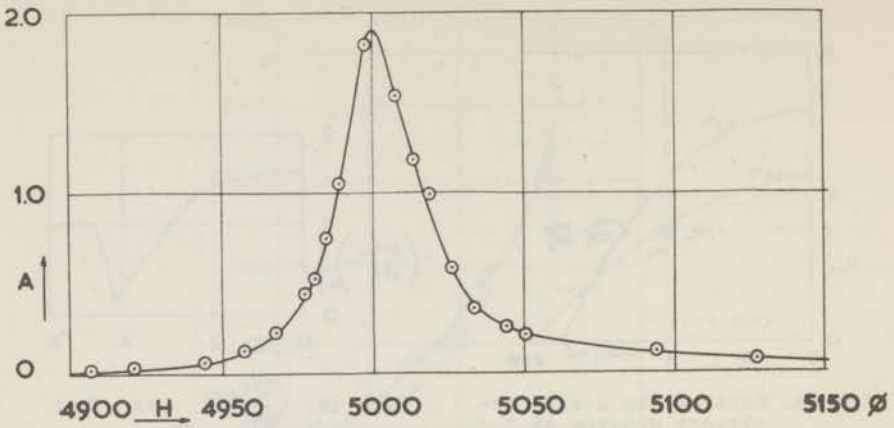

Fig. 5a^{I}. Galvanogram for the low line, H_L, at 1.4^{O}K.

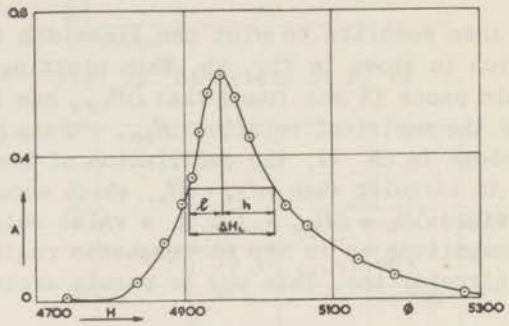

Fig. 5a^{II}. Galvanogram for the low line at 3.02^{O}K.

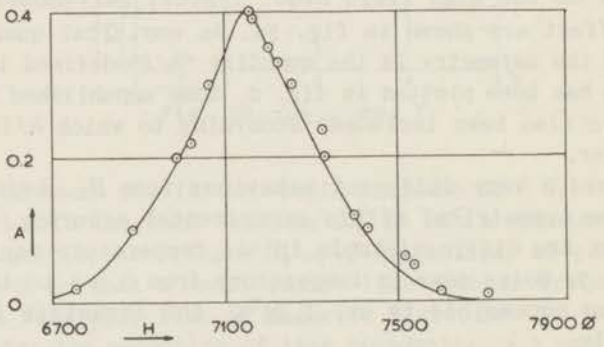

Fig. 5b^{I}. Galvanogram for the high line, H_H, at 1.36^{O}K.

account that small misorientations of the crystal produces an increase in ΔH_H above 2.3^{O}K and a decrease in ΔH_H below 2.3^{O}K.

If one computes ΔH_{Hpx} in the region below 2.3^{O}K according to the relation $H_H^2 = \alpha H_c^{*2} + H_{px}^2$, $\Delta H_{Hpx} = (H/H_{px})\Delta H_H$, then $\Delta H_{px} = 2.3\Delta H = 770\ \Phi$ at 1.3^{O}K. This emphasizes even more the rapid increase of ΔH_H as T decreases below 2.3^{O}K.

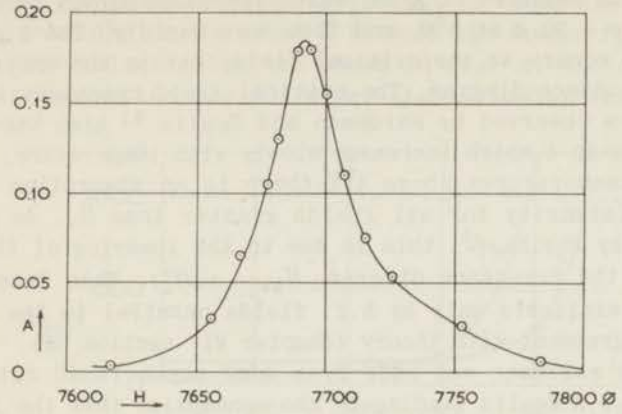

Fig. 5b[II]. Galvanogram for the high line at 3.36°K.

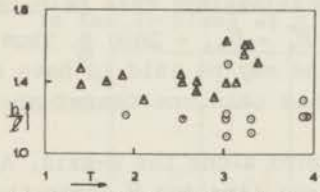

Fig. 6..Low line asymmetry, "h/l", vs. T. ○ unpublished measurements of Ubbink.

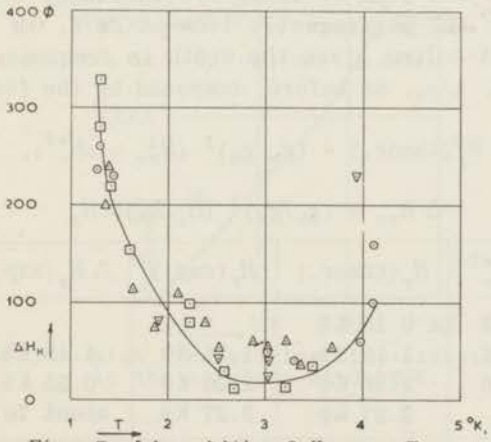

Fig. 7. Linewidth of H_H vs. T.

It may be recalled that in the region above 2.3°K the resonance H_H occurs approximately at the critical field and that the resonance diagram in the vicinity of this line is a vertical line. Thus, it doesn't make sense in this case to speak of $\Delta H_{H_{px}}$ and the observed width has to be considered as intrinsically one

of magnetic field. The behaviour of ΔH_H in this region is similar to the width measured at 8 mm, which increased slowly from ≈ 15 Φ at 1.3°K to ≈ 30 Φ at 3°K, and then more rapidly. The 8 mm resonance also occurs at the critical field, but in the upper branch of the resonance diagram. The critical field resonance at radio frequencies observed by Hardeman and Poulis [8] also has a linewidth of 20-40 Φ which increases slowly with temperature.

b. At temperatures above 4°K there is an absorption tail of constant intensity for all fields greater than H_H. As already described by Ubbink [3], this is due to the lowering of the upper branch of the resonance diagram, $H_{px} = \sqrt{a H_a^*}$). This "absorption ridge" is excitable only by h.f. fields parallel to the *a*-axis, as is in agreement with theory (chapter VI, section B2).

A rough estimate was made from some unpublished data of J. Ubbink and J.A.Poulis leading to the conclusion that the intensity of the tail at 4.16°K was about half that at 4.22°K, where the "ridge" has its maximum intensity. This is in accordance with the fact that at 4.22°K, $\sqrt{a H_a^*} = H_{px} = 3050$ Φ. Thus, since at 4.16°K, $\sqrt{a H_a^*} = 3600$ Φ, this line may be said to have a half width ΔH_{px} of about 1000 Φ. In this case one cannot speak of a ΔH since $d\omega/dH = 0$.

c. At 4.07°K H_L is zero along the *a*-axis. Above this temperature there is a resonance line for H along the *b*-axis. The only data on this line consist of two unpublished measurements of Ubbink at 4.11 and 4.22°K. These are included, together with a measurement on the paramagnetic line at 20°K, in the following table. The last column gives the width in frequency expressed in the same units, $1/\gamma_x$, as before, computed by the formulae

$$H_y^2(\text{theor.}) = (g_a/g_b)^2 \; (H_{px}^2 - a H_c^{*2}),$$

$$\Delta H_{px} = (g_b/g_a)^2 \; (H_y/H_{px}) \Delta H_y$$

T	$a H_c^{*2}$	H_y(theor.)	H_y(exp.)	ΔH_y(exp.)	ΔH_{px}
4.07°	9.3	0 10 KΦ			
4.11°	8.2	1.10 KΦ	1.16 KΦ	1.15 KΦ	370 Φ
4.22°	4.6	2.30 KΦ	2.26 KΦ	0.55 KΦ	370 Φ
20°	–	3.27 KΦ	3.27 KΦ	about 70 Φ	65 Φ

The value of $\Delta H_{px} = 370$ Φ is not very different from that for a field along the *a*-axis, which is 410 Φ at 4.07°K. The figures in the table indicate that the position and width of the line approach the paramagnetic values in a smooth way. There was some evidence that the paramagnetic line actually begins to broaden some few hundredths of a degree above 4.32°K, as was also observed at 8 mm (chapter I, section A).

B. *The resonance field in the ab- and ac-planes*

Several experiments were carried out to study the dependence of the linewidth on the angle β between the static field and the a-axis. Several examples are shown in fig. 8. Although a complete investigation was not made, the following features were observed.

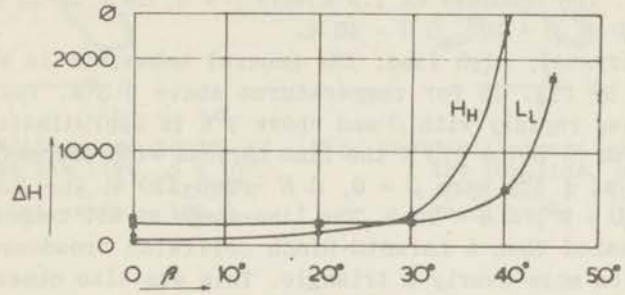

Fig. 8a. High line and low line linewidths in the ac-plane at 3.30°K.

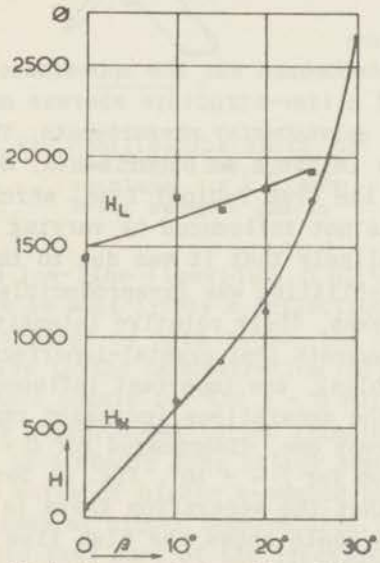

Fig. 8b. High line and low line linewidths in the ab-plane at 3.98°K.

ac-crystal, low line: for all temperatures up to 3.9°K the low line width increases 10 to 20% as β increases from zero to 25°. The line broadens more rapidly above 25°.

ac-crystal, high line: between 3.9°K and 2.5°K the high line width increases by a factor of 2 to 4 up to β = 20° and then increases more rapidly. There is only one measurement below 2.5°K, namely at 1.3°K, from which it seems that the high line first narrows with increasing β, and then increases rapidly again. The

measured values were 300 Φ, 100 Φ and 400 Φ at $\beta = 0^{o}$, 30^{o}, and 40^{o}, respectively. These quantitative values are not very reliable, however, since they depend strongly on slight misorientations toward the *b*-axis.

ab-crystal, low line: for all temperatures (up to 4^{o}K) the width increases very slowly with β until the two lines merge near $\beta = 13^{o}$. The readings at 1.3^{o}K were $\beta = 0$, ΔH = 20-25 Φ; $\beta = 7.5^{o}$ ΔH = 20 Φ; $\beta = 10^{o}$, ΔH = 40 Φ.

ab-crystal, high line: the general behaviour is well illustrated by fig. 8b for temperatures above 2.3^{o}K. The linewidth increases rapidly with β and above 3^{o}K is approximately proportional to β. Below 2.3^{o}K the line narrows with increasing β. The values at 1.3^{o}K were $\beta = 0$, ΔH = 280-330 Φ; $\beta = 3.5^{o}$, ΔH = 110 Φ; $\beta = 9^{o}$, ΔH = 90 Φ. The line-shape at all temperatures was more peaked than a Lorentz-Bloch collision broadened line. It resembled more nearly a triangle. This was also observed in the 8 mm experiments for the resonance at the critical field (chapter I, section B).

C. *Line structure*

A puzzling phenomenon was the appearance in the oscilloscope observations of a line-structure whereas no such structure was observed in the galvanometer measurements. This splitting appeared below 2^{o}K as in the 8 mm experiments. Since this effect did not appear for the free radical line, which was used for calibration, and was not influenced by varying the sweep from 50 to 150 Φ, it is unlikely that it was due to the electronics of the apparatus. The splitting was irreproducible with respect to the the number of peaks, their relative intensities, and their separations. This suggests that crystal-imperfections, such as cracks due to rapid cooling, are important influences. This agrees with the fact that the separations increased rapidly with β and, in all crystals except one, disappeared for $\beta = 0$.

The two photos for $\beta = \pm 10^{o}$, fig. 9, for the low line in the *ab*-plane show that the separation there is of the order of 10-30 Φ. The third photo shows the high line in the *ab*-plane for $\beta = 4^{o}$.

3. Remarks

The linewidth measurements reported in this chapter, supplement the detailed studies already made on the resonance diagrams ω vs. H. While the latter are fairly well explained by the molecular field models of Ubbink [1)2)] and of Yosida and Nagamiya [6)7)] there is as yet no theory for the linewidths.

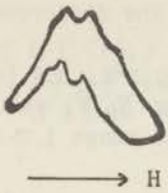

Fig. 9a. Oscilloscope photo of the low line, $\beta = 10^{o}$, ab-plane, $T = 1.30^{o}$K. Total sweep = 130 Φ.

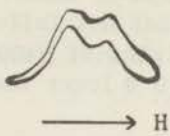

Fig. 9b. Oscilloscope photo of the low line, $\beta = -10^{o}$, ab-plane, $T = 1.30\ ^{o}$K. Total sweep = 150 Φ.

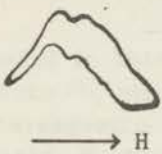

Fig. 9c. Oscilloscope photo of the high line, $\beta = 4^{o}$, ab-plane, $T = 1.30^{o}$K. Total sweep = 120 Φ.

The fact that the low-line linewidth, ΔH_L, decreases with decreasing temperature is most likely a reflection of the increasing order. In the language of spin waves, the concentration of small k-values relative to the concentration of great k-numbers is increasing. Resonance occurs for the $k = 0$ spin waves and the linewidth is inversely proportional to the lifetime of this $k = 0$ state. This lifetime is probably long at low temperatures where collisions with spin waves of higher k-number become less frequent than as is the case at higher temperatures.

It could be possible that part of the linewidth is due to the magnetic moment of the nuclear spin, which gives rise to a structure in diluted copper salts [23] with a total splitting of the order of 100 Φ.

The behaviour of the high-line linewidth, ΔH_H, below 2.3°K is astonishing, and it would be interesting to follow this linewidth to lower temperatures when the pumping equipment becomes available. We only wish to recall that there are several other puzzles that remain to be solved in connection with the high line which were described in chapter III.

Summarizing these all:

1) ΔH_H increases rapidly from 2.3 to 1.2°K.
2) ΔH_H narrows for small increasing β below 2.3°K, but broadens above 2.3°K.
3) H_H is maximal in the *ab*-plane for $\beta = 3^o$. The difference with $\beta = 0^o$ equals 120 Φ.
4) $H_H(T)$ does not follow the H_c^* curve above 2.3°K, but is about 80 Φ higher at 9400 MHz. At 32000 MHz the $H_H(T)$ values are about 40 Φ lower than the H_c^* values in the range 1.3-4°K.

Chapter VI

THEORETICAL STUDY ON THE ANTIFERROMAGNETIC ROTATOR WITH RHOMBIC SYMMETRY

As an introduction to the classical model of the antiferromagnetic rotator, the paramagnetic case will be discussed first.

1. The paramagnetic rotator

A. *Normal modes*

a. Isotropic g-value

Much of what is presented in this section, has already been treated by Bloch [19] and Pake [20], whose results I will summarize.

The torque exerted on a magnetic dipole with magnetic moment $\mathbf{M}$, placed in a magnetic field, $\mathbf{H}$, is given by $[\mathbf{M} \times \mathbf{H}]$. The rate of change of angular momentum, $\mathbf{I}$, is equal to this torque, so that:

$$\frac{d\mathbf{I}}{dt} = [\mathbf{M} \times \mathbf{H}] \qquad (1.01)$$

$\mathbf{I}$ and $\mathbf{M}$ are related by the formula

$$\mathbf{M} = \frac{g.e}{2mc}\mathbf{I}, \qquad \text{or} \qquad \mathbf{M} = \gamma\mathbf{I} \qquad (1.02)$$

γ is proportional to g and has the negative sign because of the negative charge of the electron.

For the case that g is a scalar, and $\mathbf{H} = (H_x, 0, 0)$, the solution of (1.01) becomes

$$M_y = M \cos \omega_o t; \quad M_z = M \sin \omega_o t; \quad M_x = \text{constant} \quad \text{and} \quad \omega_o = -\gamma H \qquad (1.03)$$

(M is an arbitrary constant)

ω_o, the frequency of precession, will be considered as a positive quantity. (1.03) means that the precession is such that the sense of the rotation and the direction of the external magnetic field are related to each other by the right hand screw rule. As will be shown in the next section, a small magnetic field precessing around the x-direction in the same sense as the magnetization vector will give rise to absorption of energy.

b. Anisotropic g-value

In this case the relation between $\mathbf{M}$ and $\mathbf{I}$ is

$$M_x = \gamma_x I_x; \quad M_y = \gamma_y I_y; \quad M_z = \gamma_z I_z, \tag{1.04}$$

where the coordinate-axes are taken as the principal axes of the g- or γ-tensor. The magnetic energy in this case is $W_H = -(\mathbf{M}.\mathbf{H}) = -\Sigma_k \gamma_k I_k H_k$. As was first pointed out by Ubbink [3] (page 35), this is identical to the energy of a magnetic moment, $\mathbf{I}$, placed in a field with components $\gamma_k H_k$. When equation (1.01) is applied to $\mathbf{I}$, this gives:

$$\frac{dI_y}{dt} = I_z \gamma_x H_x; \quad \frac{dI_z}{dt} = -I_y \gamma_x H_x; \quad \frac{dI_x}{dt} = 0 \tag{1.05}$$

The solution is $M_y = \gamma_y I_y = I\gamma_y \cos\omega_o t$, $M_z = I\gamma_z \sin\omega_o t$ and $\omega_o = -\gamma_x H_x$. The motion is no longer circular, but there is an elliptical precession of the magnetic moment with major axis in the direction of the greater g-value.

B. *Complex susceptibility*

The complex notation simplifies the calculation of the absorption and dispersion and a definition of the symbols to be used will be given. The following quantities will be introduced:

$$\delta\mathbf{H}(t) = \mathrm{Re}\,[\mathbf{h}\exp(i\omega t)]$$

$$\delta\mathbf{M}(t) = \mathrm{Re}\,[\mathbf{m}\exp(i\omega t)] = \mathrm{Re}\,[\chi\mathbf{h}\exp(i\omega t)] \tag{1.06}$$

$\mathbf{h}$ can be taken as a complex magnetic field, e.g. as: $h_y - ih_z$ This case represents a circularly polarized magnetic field, namely,

$$\delta\mathbf{H}(t) = \mathrm{Re}[(h_y - ih_z)(\cos\omega t + i\sin\omega t)] = h_y\cos\omega t + h_z\sin\omega t.$$

Since I am only interested in the interpretation of the experiments done with linearly polarized light, I put $\delta\mathbf{H}(t) = \mathbf{h}\cos\omega t$ where $\mathbf{h}$ is real.

After introducing χ, the expression for the magnetic moment becomes

$$\delta\mathbf{M}(t) = \mathrm{Re}[\chi' - i\chi'')\mathbf{h}(\cos\omega t + i\sin\omega t)] = \mathbf{h}\chi'\cos\omega t + \mathbf{h}\chi''\sin\omega t.$$

It should be kept in mind that in general both χ' and χ'' are tensors.

As an example of a calculation with complex numbers, the normal modes in the anisotropic case will be calculated.

Assuming as the solution of (1.05): $\delta I_y(t) = \mathrm{Re}[i_y.\exp(i\omega t)]$ and $\delta I_z(t) = \mathrm{Re}[i_z.\exp(i\omega t)]$, (1.05) can be rewritten as $i\omega i_y = -\omega_o i_z$ and $i\omega i_z = \omega_o i_y$, where the i_k are complex and ω_o stands for: $-\gamma_x.H_x$. The result is $\omega = \omega_o$ and $i_y = ii_z$.

The solution one gets by considering the real parts is, $\delta I_y(t) = i\cos\omega_o t$ and $\delta I_z(t) = i\sin\omega_o t$, aside from an unimportant phase angle. This leads to the same values for the magnetic moment as have been derived in section 1.

C. *Resonance absorption*

a. Isotropic g-value

The situation to be considered will be the following: A static magnetic field is applied along the x-axis, $\mathbf{H} = H_x$. At the same time a high frequency magnetic field will be applied along the y-axis, $H_y = h\cos\omega t = h\,\mathrm{Re}[\exp(i\omega t)]$. The introduction of these magnetic field components in equation (1.01) and (1.02) gives rise to expressions for m_y and m_z in which there are factors $\omega^2 - \omega_o^2$ in the denominators. When $\omega = \omega_o$, the frequency of the oscillating magnetic field equals the precession frequency, and the magnetic moments, m_k, become infinite. In order to overcome this difficulty and to be able to derive formulae applicable to the experimentally observed dispersion and absorption of the high frequency energy, damping terms must be introduced into formula (1.01). Two different ways of introducing damping terms will be considered. The equations without damping terms, arising from (1.01) are

$$\frac{d\delta M_x}{dt} = -\gamma\delta M_z h\cos\omega t$$

$$\frac{d\delta M_y}{dt} = \gamma H\delta M_z \qquad (1.07)$$

$$\frac{d\delta M_z}{dt} = \gamma M_x h\cos\omega t - \gamma H\delta M_y$$

where, $H_x = H$; $H_y = h\cos\omega t$; $H_z = 0$; χ_o = static susceptibility $= \frac{M_x}{H_x}$; $\omega_o = -\gamma H$ and $M_k = M_{ok} + \delta M_k(t) = M_{ok} + m\{\cos(\omega t + \phi)\}$.
This gives, neglecting second order terms,

$$M_x = \text{constant} = \chi_o H,$$

$$\frac{d^2\delta M_y}{dt^2} + \omega_o^2\,\delta M_y = \omega_o^2\,\chi_o h\cos\omega t$$

$$\frac{d^2\delta M_z}{dt^2} + \omega_o^2\,\delta M_z = \omega\omega_o\chi_o h\sin\omega t$$

α. Friction damped magnetic oscillator

One of the ways in which damping can be brought in, is to introduce in both equations a term $\frac{1}{t}\frac{d\delta\mathbf{M}}{dt}$. This then leads to the equations of motion of a friction damped harmonic oscillator of which the solution is easily obtained by putting

$$\delta\mathbf{M}(t) = A\exp(i\omega t) + Bi\exp(i\omega t),$$

in which A en B are real.

$$\delta M_y(t) = \frac{\omega_o^2 \chi_o h}{(\omega_o^2 - \omega^2)^2 + \frac{\omega^2}{t_1^2}} \{(\omega_o^2 - \omega^2)\cos\omega t + \frac{\omega}{t_1}\sin\omega t\} \qquad (1.08)$$

The last term is 90° out of phase with the high frequency magnetic field and is thus responsible for absorption (see later). I will not consider the term that is in phase, because in our experiments only absorption and no dispersion was measured.

Using the definition of section 2 for χ'', one gets:

$$\chi_y'' = \frac{\chi_o \omega_o^2 \omega t_1}{t_1^2(\omega_o^2 - \omega^2)^2 + \omega^2} \qquad (1.09)$$

For the z-component there will be no absorption, because the high frequency magnetic field has no component in that direction.

The χ_y'' vs ω curve has a maximum at

$$\omega_{peak} = \sqrt{\omega_o^2 - \frac{1}{t_1^2}}$$

The frequency difference, $\Delta\omega$, between points, where χ_y'' has half the value of the maximum is equal to $1/t_1$ if $\Delta\omega \ll \omega_o$. This condition was fulfilled for the lines that were studied. In this case (1.07) can be reduced to

$$\chi_y'' = \frac{\chi_o \omega_o \Delta\omega}{4(\omega_o - \omega)^2 + \Delta\omega^2} \qquad (1.10)$$

For the peak value of χ_y'' this gives:

$$\chi_{peak}'' = \frac{\chi_o \omega_o}{\Delta\omega}$$

Now the absorption per second is equal to:

$$A_{sec} = \frac{\omega}{2\pi}\int_{t=o}^{t=2\pi/\omega} (\delta\mathbf{H}\,\frac{d\delta\mathbf{M}}{dt})dt$$

With the introduction of χ'' this integral reduces to

$$A_{sec} = \frac{h^2 \omega \chi''}{2} \qquad (1.11)$$

The peak absorption then becomes

$$A_{\substack{peak \\ sec}} = \frac{h^2 \omega_o^2 \chi_o}{2\Delta\omega} \qquad (1.12)$$

Another way of looking at this problem is to put $\delta H_y(t) = h_y \cos\omega t$ equal to

$$\delta H_y(t) = (0, \tfrac{1}{2}h\cos\omega t, \tfrac{1}{2}h\sin\omega t) + (0, \tfrac{1}{2}h\cos\omega t, -\tfrac{1}{2}h\sin\omega t).$$

The first term represents a magnetic field vector rotating in the same sense as the magnetic moments. This vector can give resonance absorption, while the other, left circularly polarized magnetic field vector is far off resonance. In this picture the same expression for the intensity of the absorption will be found but the y- and z-directions now each contribute half.

The physical model on which this formalism is based, pictures the spin as rotating in a viscous fluid.

β. Collision damped magnetic oscillator

In another physical model, given by F.Bloch [19] for the case of nuclear resonance phenomena, the time variation of the macroscopic sum vector of the magnetic moments is studied. Two relaxation times t_1 and t_2 play an important role in this theory.

Relaxation time t_1. When a magnetic field is switched on in the x-direction, one can ask how the component of the magnetic moment in that direction, M_x, will approach its equilibrium value: $M_o = \chi_o H_x$. Bloch assumed an exponential approach, so that the equation is

$$\frac{dM_x}{dt} = \frac{M_o - M_x}{t_1}$$

with the solution $M_x = M_o(1 - \exp\text{-}t/t_1)$

t_1 is called the spin-lattice relaxation time and is short when the contact between spin and lattice is strong.

Relaxation time t_2. In the y- end z-direction there is no magnetization, at equilibrium. Bloch assumed, that when a component of the magnetization is present in a direction perpendicular to the static field H_x, this magnetization will die out when no h.f. magnetic field is present according to:

$$\frac{dM_y}{dt} = \frac{-M_y}{t_2}$$

with the solution $M_y = M_{oy} \exp(-t/t_2)$

The initial y- or z-component of the sum vector represents a phase coherence between the y- or z-components of the individual spins. The exponential decay of this phase relationship is ascribed to the following mechanisms.

a) Each individual spin is surrounded by neighbouring spins, distributed at random parallel or antiparallel with respect to the magnetic field **H**. This causes an internal magnetic field, $\mathbf{H}_i$, which must be added to the field **H** for some spins and substracted for other spins. Because of the relation $\omega = \gamma(H \pm H_i)$, the precession frequency will not be the same for different spins. This is one reason why an initial phase relation gets lost after some time.

b) Another phase disturbing mechanism is the so called spin-spin relaxation. If one spin is parallel to the static field and its neighbour is antiparallel, there is a probability that these spins will flop each other over, so that the total energy remains the same. The situation now is reversed with respect to the spins and the result is again a loss of the phase relationship.

A quantummechanical way of looking at the spin-spin relaxation is to consider the spin-spin interaction as a lifetime limiting process, with a consequent broadening of the energy levels. Using Heisenberg's uncertainty relation, the broadening ΔE is given by: $\Delta E \approx \hbar/t_2$. Since $E = \hbar\omega$, this results into $\Delta E/E \approx 1/\omega t_2$. There will be a region, $\Delta\omega$, of frequencies, for which resonance occurs where $\Delta\omega \approx 1/t_2$.

A high frequency field $\delta\mathbf{H}$ tends to create a high frequency magnetic moment according to: $\delta\mathbf{M} = \chi_{h.f.}\delta\mathbf{H}$, but t_2 tends to destroy that magnetic moment. It is the competition between these tendencies that results into a $\chi_{h.f.}$ which is finite and is responsible for the linewidth of the absorption vs. ω curve.

The equations (1.07) including Bloch's damping terms are

$$\begin{aligned} \frac{d\delta M_x}{dt} &= -\gamma \delta M_z h\cos\omega t + \frac{(M_o - M_x)}{t_1} \\ \frac{d\delta M_y}{dt} &= \gamma H \delta M_z - \frac{\delta M_y}{t_2} \\ \frac{d\delta M_z}{dt} &= \gamma M_x h\cos\omega t - \gamma H \delta M_y - \frac{\delta M_z}{t_2} \end{aligned} \qquad (1.13)$$

calculating χ''_y from these equations one obtains

$$\chi''_y = \tfrac{1}{2}\chi_o \omega_o t_2 \frac{1}{1 + t_2^2(\omega_o - \omega)^2 + \gamma^2 h^2 t_1 t_2} \qquad (1.14)$$

Bloch obtained this formula by decomposing the linearly polarized h.f. field into a right and a left circularly polarized field as was done in section α and then neglecting the influence of the left circularly component. This assumption, which is only valid for narrow lines, will be investigated more thoroughly later on. With respect to the formula two cases are of importance.

1) $\gamma^2 h^2 t_1 t_2 \ll 1$.

This condition can always be fulfilled when the h.f. magnetic field is sufficiently weak, even if t_1 or t_2 happens to be long. In that case the χ'' versus ω curve has a Lorentz shape with $\Delta\omega = 2/t_2$, where $\Delta\omega$ signifies the frequency difference between points where χ'' equals $\frac{1}{2}\chi''_{peak}$. The expression for χ'' is then identical with equation (1.10) for the friction damped oscillator.

2) $\gamma^2 h^2 t_1 t_2 \geq 1$.

In this case one speaks about saturation effects and the physical meaning is, that the h.f. field which always acts in such a way as to equalize the populations of the different spin-states, now induces transitions faster than the contact between the spin-system and the thermal bath can establish the equilibrium difference in populations. This is manifested in a reduction of the net magnetization, an effect which can also be described in terms of a heating up of the spin-system by the h.f. energy input. There are several effects associated with the saturation namely:

a) When the intensity of the h.f. field imposed on the sample is increased by a factor of n, the energy absorbed will increase by less than a factor n. For very high h.f. power, the energy absorbed per sec., $\frac{1}{2}h^2\omega\chi''$, approaches the value $H^2\chi_o/4t_1$.

b) The resonance line broadens with increasing h.f. intensity, so that e.g. when $\gamma^2 h^2 t_1 t_2 = 1$, one finds that $\Delta\omega = 2.8/t_2$.

In the paramagnetic and in the antiferromagnetic resonance experiments described in Ch.IV and V, these effects were avoided because the radiation-power, about 10^{-6} Watt, was sufficiently low. Therefore the case of saturation will not be considered.

Bloch's assumption that the circular component, having opposite sense to the precession of the magnetization vector, is far off resonance and thus may be neglected, is only true for $\Delta\omega \ll \omega_o$. The general expression for χ''_y, assuming only $\gamma^2 h^2 t_1 t_2 \ll 1$, is obtained by solving formulae (1.13), using complex calculation, This leads to

$$(i\omega + 1/t_2)m_y + \omega_o m_z = 0$$

$$-\omega_o m_y + (i\omega + 1/t_2)m_z = \gamma M_x h_y$$

where $$M_x = \chi_o H.$$

The solution for the imaginary part of the susceptibility equals

$$\chi''_y = \frac{\chi_o \omega_o t_2}{1 + t_2^2(\omega_o - \omega)^2} \cdot \frac{2\omega\omega_o}{1/t_2^2 + (\omega_o + \omega)^2} \qquad (1.15)$$

Bloch's formula (1.14) has been derived by neglecting the left circularly polarized component of the magnetic field. The formula – when omitting the saturation term – is only identical with (1.15) when the last term in (1.15) is put equal to ½. This approximation has only a small influence on the line-shape even for lines so broad that $\Delta\omega \approx \frac{1}{4}\omega_o$, as can easily be verified. For the lines encountered in Ch.V, $\Delta\omega$ was $\leq$ 1/10 ω_o in nearly all the cases.

Summarizing:

Bloch's equation of motion for paramagnetism is

$$\frac{d\mathbf{M}}{dt} = \gamma[\mathbf{M}\times\mathbf{H}] - \frac{(\mathbf{M} - \mathbf{M}_o)}{t} \qquad (1.16)$$

Assuming as usual $\mathbf{H} = (H_x;\ h_y \exp i\omega t;\ h_z \exp i\omega t)$

$$\mathbf{M} = (M_x;\ m_y \exp i\omega t;\ m_z \exp i\omega t)$$

where $M_x = \chi_o H_x$ and $t = t_1$ when dM_x/dt is considered and $t = t_2$ when dM_y/dt or dM_z/dt is considered.

Introduction of the oscillatory parts of $\mathbf{H}$ and $\mathbf{M}$ in (1.16) leads to

$$\mathbf{m}(i\omega + \frac{1}{t_2}) = \gamma[\mathbf{M} \times \mathbf{h}] + \gamma[\mathbf{m} \times \mathbf{H}] \qquad (1.17)$$

identisch met (1.10)

This led to $$\chi'' = \frac{\chi_o \omega_o \Delta\omega}{4(\omega_o - \omega)^2 + \Delta\omega^2}$$

so that $$\chi''_{peak} = \frac{\chi_o \omega_o}{\Delta\omega}$$

and $$A_{sec} = \tfrac{1}{2}h^2\omega\chi''$$

so that $$A_{\substack{peak \\ sec}} = \frac{\chi_o \omega_o^2 h^2}{2\Delta\omega}$$

Approximations made: No saturation effects; $\Delta\omega \ll \omega_o$.

γ. It is known that for very broad lines the description of Bloch leads to wrong conclusions. In order to obtain a satisfactory description of relaxation phenomena, where $1/t \gg \omega_o$ the theory of collision broadening was refined by Fröhlich, Van Vleck and Weiskopff [22)34)]. In the description of the antiferromagnetic resonance the formalism of Bloch has been chosen for the following reasons:

The resonance lines encountered are all rather narrow, so that the different descriptions lead practically to the same result.

The second reason is that no theory exists for antiferromagnetic linewidths and if such a theory would be developed, it is likely that the mechanisms of line-broadening will be different from those encountered in paramagnetic resonance. Bloch's treatment applied to antiferromagnetic resonance has the advantage to give the simplest possible formalism with which it was possible to account for the observed absorption intensities under the different experimental conditions.

For these reasons I will not treat the theory of Fröhlich, Van Vleck and Weiskopff.

b. Anisotropic g-value

The situation in which the g-tensor has orthorhombic symmetry will now be considered, because this is in fact the case for $CuCl_2.2H_2O$. In the paramagnetic region the principal axes of the g-tensor ellipsoid coincide with the crystal axes and are (see Ch. I) $g_a = 2.187$; $g_b = 2.037$; $g_c = 2.252$.

The equation of motion for the angular momentum vector is $\frac{d\mathbf{I}}{dt} = [\mathbf{I} \times (\gamma \mathbf{H})]$. Introducing an anisotropy in the damping term t_2 as t_{2y} and t_{2z} and using the relation $M_k = \gamma_k I_k$, one obtains by solving the equation for χ, using Bloch's formalism

$$\chi_y = \frac{\gamma_y^2}{\gamma_x^2} \chi_{ox} \frac{\omega_o^2}{\omega_o^2 + (i\omega + 1/t_{2y})(i\omega + 1/t_{2z})} \qquad (1.18)$$

For narrow lines and when writing g_y/g_x instead of γ_y/γ_x, this leads to

$$\chi_y'' = \frac{g_y^2}{g_x^2} \chi_{ox} \frac{\omega_o \Delta\omega}{4(\omega_o - \omega)^2 + \Delta\omega^2} \qquad (1.19)$$

where $$\Delta\omega = \frac{1}{t_{2y}} + \frac{1}{t_{2z}}$$

The expression for χ_z'' is obtained by replacing y by z in the above formula. It thus turns out that the h.f. susceptibility is proportional to the square of the g-value in that direction. The same dependence on the g-value is valid for the static susceptibility:

$$\chi_{ok} = \frac{g_k^2 \mu_o^2 N}{4kT}$$

The dependence of the absorption intensity on the square of the g-value was checked by measurements on $K_3(Fe^{0.1}, Co^{0.9})(CN)_6$ at 20^oK. This crystal is very anisotropic and the g-values along the axes are: 2.3; 2.2 and 0.9, which is in agreement with meas-

urements of Bleaney and Ingram [21]. It was observed that the intensity of the absorption when the h.f. field was in the (g = 2.3) direction was about 6 times that for the h.f. field along the (g = 0.9) direction. In this experiment the constant field was oriented in the (g = 2.2) direction.

D. *Quantum mechanical treatment of absorption*

A quantum mechanical derivation will be given from which follows the dependence of the absorption on the angle between **H** and **h** and on the g-value. It will be assumed that S = ½.

The quantum mechanical condition for resonance absorption is: The energy quanta of the r.f. field, $h\nu$, must equalize the energy difference 2(**MH**) between the two eigen states characterized for each individual spin by S = -½ and S = +½, where $\mathbf{M} = g\mu_o\mathbf{H}/2$ and μ_o is the Bohr magneton. This leads to the equation for the resonance absorption $h\nu = \hbar\omega = g_x\mu_o H_x$, which is identical to (1.03), since $\gamma = g\mu_o/\hbar$.

The intensity of the resonance absorption is proportional to the transition probability $+½ \rightarrow -½$, so that with perturbation theory one gets

$$A_{sec} = C\left|\langle\psi^*_{-½}\ (\mathbf{M}_{op}.\mathbf{H}_{op})\ \psi_{+½}\rangle\right|^2$$

Now $(\mathbf{M}_{op}.\mathbf{H}_{op}) \sim h(g_x\cos\zeta I_{x_{op}} + g_y\sin\zeta\cos\beta I_{y_{op}} + g_z\sin\zeta\sin\beta I_{z_{op}})$,

where ζ denotes the angle between **h** and the x axis and β is the angle between the projection of **h** on the yz plane and the y axis. I_{op} stand for the operator of angular momentum.

From the properties of the Pauli spin matrices, it follows that

$$\langle\psi^*_{-½}|I_{x_{op}}|\psi_{+½}\rangle = 0$$

$$\langle\psi^*_{-½}|I_{y_{op}}|\psi_{+½}\rangle = ½$$

$$\langle\psi_{-½}|I_{z_{op}}|\psi_{+½}\rangle = -½i$$

It therefore follows that:

$$A_{sec} = Ch^2\sin^2\zeta\left|g_y\cos\beta - ig_z\sin\beta\right|^2 = Ch^2\sin^2\zeta(g_y^2\cos^2\beta + g_z^2\sin^2\beta).$$

The same dependence is thus found as was derived by classical theory.

2. The antiferromagnetic rotator

A. *Introduction and equation*

In order to discuss the resonance measurements, the argument made in chapter II may be repeated. The theory of Ubbink based on the static model of Gorter and Haantjes is applicable in the case of very low temperature for any value of the static magnetic field. The theory of Yosida, however, based on the static model of Nagamiya is more useful when temperature effects are discussed and the static fields applied are only moderately strong with respect to the exchange field. As the influence of temperature on the polarization was investigated in the experiments described in Chapter IV, the theory of Yosida has been applied, except for a correction of the anisotropy of the g-values as will be discussed later.

The equation of motion for antiferromagnetic resonance has been discussed by several authors [15) 24) 3) 6)]. The lattice is divided into two sublattices with opposite spin directions. The exchange interaction between the so called + and – spins can be described by a magnetic field, the exchange field, which has the tendency to align the spins antiparallel to each other. This exchange field is supposed to be anisotropic, such that it is strongest in the *a*-direction and weakest in the *c*-direction.

The individual spins in the two sublattices can be added, leading to two macroscopic spins, denoted by $\mathbf{M}^+$ and $\mathbf{M}^-$. The torques appearing in the equation of motion consists of:

a) The torque arising from the exchange field, $\mathbf{AM}^{\mp}$, $-[\mathbf{M}^{\pm} \times \mathbf{AM}^{\mp}]$.

b) The torque arising from the anisotropy field. Its components are,

$$-\frac{(K_2 - K_1)}{M_o^2} M_z^{\pm} M_y^{\pm} \; ; \quad \frac{K_2}{M_o^2} M_x^{\pm} M_z^{\pm} \; ; \quad -\frac{K_1}{M_o^2} M_x^{\pm} M_y^{\pm}$$

where

$$\frac{K_1}{M_o} = H_{ex}(a) - H_{ex}(b)$$

and

$$\frac{K_2}{M_o} = H_{ex}(a) - H_{ex}(c)$$

where $H_{ex}(a)$ denotes the exchange field when the spins are aligned in the *a*-direction etc.

c) The torque arising from the external magnetic field, $\mathbf{H} = \mathbf{H}_o + \delta\mathbf{H} = \mathbf{H}_o + \mathbf{h}\exp(i\omega t)$. This torque is: $[\mathbf{M}^{\pm} \times \mathbf{H}]$.

The subscript in $\mathbf{H}_o$ will be left out from the equations for the sake of brevity, unless confusion might occur.

This leads to the equation of motion given by Yosida ref. [6)]. The equation will be supplied here with damping terms as used by

Bloch for the case of paramagnetic resonance described in (1.16).. One obtains the formula:

$$\frac{1}{\gamma}\frac{d\mathbf{M}^{\pm}}{dt} = \mathbf{M}^{\pm} \times (\mathbf{H} - A\mathbf{M}^{\mp}) +$$

$$+ \left[\frac{-(K_2 - K_1)}{M_o^2} M_z^{\pm}M_y^{\pm}, \frac{K_2}{M_o^2} M_x^{\pm}M_z^{\pm}, \frac{-K_1}{M_o^2} M_x^{\pm}M_y^{\pm}\right] - \frac{(\mathbf{M}^{\pm} - \mathbf{M}_{st}^{\pm})}{\gamma t}$$

$\mathbf{M}_{st}^{\pm}$ stands for the static value of $\mathbf{M}^{\pm}$.

From this equation the equation of motion for the oscillatory part of $\mathbf{M}^{\pm}(t)$, $\delta\mathbf{M}^{\pm}$, is obtained where $\mathbf{M}^{\pm}(t) = \mathbf{M}_{st}^{\pm} + \delta\mathbf{M}^{\pm}$ as:

$$\frac{1}{\gamma}\frac{d\delta\mathbf{M}^{\pm}}{dt} = \delta\mathbf{M}^{\pm} \times (\mathbf{H} - A\mathbf{M}^{\mp}) + \mathbf{M}^{\pm} \times (\delta\mathbf{H} - A\delta\mathbf{M}^{\mp}) +$$

$$+ \left[-\frac{K_2 - K_1}{M_o^2}(\delta M_z^{\pm}M_y^{\pm} + M_z^{\pm}\delta M_y^{\pm}); \frac{K_2}{M_o^2}(\delta M_x^{\pm}M_z^{\pm} + M_x^{\pm}\delta M_z^{\pm}); \right. \quad (2.01)$$

$$\left. -\frac{K_1}{M_o^2}(\delta M_x^{\pm}M_y^{\pm} + M_x^{\pm}\delta M_y^{\pm})\right] - \frac{1}{\gamma}\frac{\delta\mathbf{M}^{\pm}}{t}$$

It is assumed in this formula that no saturation effects occur, so that the static magnetization remains unchanged when a h.f. field $\delta\mathbf{H}$ is applied so that $\frac{\mathbf{M}^{\pm} - \mathbf{M}_{st}^{\pm}}{t}$ reduces to $\frac{\delta\mathbf{M}^{\pm}}{t}$, independent whether $\mathbf{M}_{st}^{\pm}$ is zero or not.

As far as the absorption is concerned, the important quantity is: $\delta\mathbf{H}(\delta\mathbf{M}^{+} + \delta\mathbf{M}^{-}) = \delta\mathbf{H}\delta\mathbf{M}$ using Yosida's notation namely, $\mathbf{M}^{+} + \mathbf{M}^{-} = \mathbf{M}$ and $\mathbf{M}^{+} - \mathbf{M}^{-} = \mathbf{M}'$. Therefore the equation (2.01) will be transformed into two equations one for the sum vector, $\delta\mathbf{M}$, and the other for the difference vector, $\delta\mathbf{M}'$. Writing $\delta\mathbf{M} = \mathbf{m}\exp(i\omega t)$, $\delta\mathbf{M}' = \mathbf{m}'\exp(i\omega t)$ and $\delta\mathbf{H} = \mathbf{h}\exp(i\omega t)$ while the anisotropy fields K_1/M_o and K_2/M_o are neglected compared with the exchange field AM_o one obtains

$$\frac{1}{\gamma}(i\omega + 1/t)\mathbf{m} = (\mathbf{m} \times \mathbf{H}) + (\mathbf{M} \times \mathbf{h}) + \left[-\frac{K_2 - K_1}{2M_o^2}(M_y'm_z' + M_z'm_y'); \right.$$

$$\left. \frac{K_1}{2M_o^2}(M_z'm_x' + M_x'm_z'); -\frac{K_1}{2M_o^2}(M_y'm_x' + M_x'm_y')\right]$$

and $$\frac{1}{\gamma}(i\omega + 1/t)\mathbf{m}' = \mathbf{m}' \times (\mathbf{H} - A\mathbf{M}) + \mathbf{M}' \times (\mathbf{h} - A\mathbf{m}) \quad (2.02)$$

The antiferromagnetic h.f. susceptibility will be defined as

$$\chi_k = (\delta M_k^{+} + \delta M_k^{-})/\delta H_k = m_k/h_k$$

The static quantities in (2.02) will be given for the case that $\mathbf{H}$ lies in the ab-plane, making an angle β with the a-axis. The angle between the direction of the magnetic moments, $\mathbf{M}'$, and

the a-axis will be denoted by ψ, and $\chi_{\parallel}$ and $\chi_{\perp}$ are the parallel and perpendicular susceptibility. According to Yosida [6] one has

$$M_x = \chi_{\parallel} H\cos\psi\cos(\psi-\beta) + \chi_{\perp} H\sin\psi\sin(\psi-\beta)$$

$$M_y = -\chi_{\parallel} H\cos\psi\sin(\psi-\beta) + \chi_{\perp} H\sin\psi\cos(\psi-\beta)$$

$$M'_x = 2M_o\cos(\psi-\beta)$$

$$M'_y = -2M_o\sin(\psi-\beta) \qquad (2.03)$$

$$H_x = H\cos\beta \quad \text{and} \quad H_y = H\sin\beta \quad \text{while} \quad M_z = M'_z = H_z = 0$$

The symbols used have already been discussed by Yosida and Ubbink, but they are tabulated at the end of this section and compared with each other for the sake of completeness. The formulae of Yosida can be used throughout this chapter, but a special meaning has to be given to them, in order to take the anisotropy of the g-factor into account, in the way pointed out in column 2 of the table.

The development of the theoretical ideas in this chapter will be as follows:

In section B a discussion will be given of the normal mode problem in the case that **H** is oriented along the a-axis. It is proved in general that when m_k for the normal mode equals zero, a h.f. field in that direction, h_k, will not give rise to absorption.

Section C deals with χ for the case that **H** is parallel to the a-axis and χ is studied as a function of the direction of **h** and of temperature. A subdivision of this section had to be made, according to the different resonance conditions. Ca) The low line case. $H_{res} < H_c^*$. Cb) The high line case. $H_{res} > H_c^*$ and Cc) The orientation resonance. $H_{res} = H_c^*$. Here H_c^* signifies the threshold field at the temperature considered. In this section the intensity of the resonance lines is studied theoretically as a function of temperature and the direction of **h**, while the line-width measurements of Ch. V were used in some of the calculations.

Section D deals with the nodal angle experiments and a theory has been developed based on a normal mode property.

Table of symbols

Yosida's symbol as written in the formulae	Symbol corrected for g-tensor	Ubbink's formalism	Physical meaning of the symbol
H_k	$(g_k/2)H_k$	h_k/μ_k	k-component of magnetic field
h_k	$(g_k/2)h_k$	----	amplitude of h.f. field in k-direction
$\omega/\gamma = -(g_a/2)H_{px}$	----	----	resonance field for $g = 2$
----	------	$\epsilon/\mu_x = H_{px}$	= reson. field for $g = g_a$
$2AK_1$	$(g_a/2)^2\alpha H_c^{*2}$;	$c^2/\mu_x^2 = H^2_{ex}(a) - H^2_{ex}(b) = \alpha H_c^{*2}$	
$2AK_2$	$(g_a/2)^2\alpha H_b^{*2}$;	$b^2/\mu_x^2 = H^2_{ex}(a) - H^2_{ex}(c) = \alpha H_b^{*2}$	
$2A(K_2-K_1)$	$(g_a/2)^2\alpha H_a^{*2}$;	$a^2/\mu_x^2 = H^2_{ex}(b) - H^2_{ex}(c) = \alpha H_a^{*2}$	
AM		$\gamma_1/\mu_x = H_{ex}(a)$	= exchange field in the direction of the a-axis
A		$1/\chi_\perp$	
M_o		μ_k	Magnetic moment when H = 0
m_k	$(2/g_k)m_k$		Amplitude of the oscillatory part of the magnetization.
α		$\alpha = (1 - \frac{\chi_\parallel}{\chi_\perp})$	

Example: Resonance condition for H // b-axis.
Yosida: $(\omega/\gamma)^2 = 2AK_1 + H_y^2$, and Ubbink: $\epsilon^2 = c^2 + h_2^2$. Correcting Yosida's formula and dividing Ubbink's formula by μ_x, brings them both into the form of $H_{px}^2 = \alpha H_c^{*2} + (g_b/g_a)^2 H_y^2$, where H_y is the experimental resonance field along the y-axis and H_{px} the field at which para-magnetic resonance would occur when H is along the a-axis.

The correction for m_k needs some explanation. According to section 1 (1.18) for the case of anisotropic g-value in paramagnetic resonance one obtains $\chi_k^2 = (g_k/2)^2\chi_{is}$, where χ_{is} stands for the χ of an isotropic g tensor with $g = 2$. Writing $m_k = \chi_{is}h_k$, it is clear that the correction for the g-value reduces this to $(2/g_k)m_k = \chi_{is}h_k(g_k/2)$ so that $\chi_k = m_k/h_k$ now becomes $\chi_k = (g_k/2)^2\chi_{is}$. Because this factor due to $g \neq 2$ originates from the relation $M_k = \gamma_k I_k$, it enters in the same way in the formulae for paramagnetic as for antiferromagnetic resonance namely as: $\chi_k^2 = (g_k/2)^2\chi_{is}$.

B. *Normal modes; resonance condition*

By putting $\mathbf{h} = 0$ in the equation 2.02 one obtains the formula 12 of Yosida [6], repeated in section D of this chapter. The six linear equations for m_{xyz}, m'_{xyz} can only have non vanishing solutions for the m_k, m'_k when the determinant of the coefficients of m_k, m'_k equals zero. This condition gives a relation between ω/γ and $\mathbf{H}$, the resonance condition. At the same time it is possible to calculate the ratio's of the m_k and m'_k's which is simply done by taking the ratio's of the respective minors. Two cases will be considered for the situation: $\mathbf{H}$ parallel to a-axis.

a) $H < H_c^*$. One has $\beta = 0$ and $\psi = 0$. This reduces (2.03) to $M_x = \chi_{\parallel} H$. $M'_x = 2M_o$ and $H_x = H$, while the other terms are zero. One can put these expressions into (2.02) together with $\mathbf{h} = 0$. This gives $m_x = m'_x = 0$. The ratio of m_y/m_z can be obtained by taking the ratio of the minors. This can be done in two different ways, depending on which row is used. The two expressions are identical since the resonance condition, obtained by putting the determinant equal to zero applies

$$0 = (\omega/\gamma)^4 - (\omega/\gamma)^2[H^2(1+a^2) + 2A(K_1+K_2)] + (2AK_1 - aH^2)(2AK_2 - aH^2)$$

One gets:

$$\frac{m_y}{m_z} = \underbrace{\frac{i|\omega/\gamma|}{H} \cdot \frac{(\omega/\gamma)^2 - 2AK_1 - a^2H^2}{(\omega/\gamma)^2 + a2AK_1 - a^2H^2}}_{\text{I}} = \underbrace{\frac{-iH}{|\omega/\gamma|} \cdot \frac{a2AK_2 - a^2H^2 + (\omega/\gamma)^2}{2AK_2 + a^2H^2 - (\omega/\gamma)^2}}_{\text{II}}$$

Now the resonance diagram (ω vs. $\mathbf{H}$) consists of two branches as is shown in Ch.II fig. 1. In the high frequency branch one has $|\omega/\gamma| \geq \sqrt{2AK_2}$ and in the low frequency branch $|\omega/\gamma| \leq \sqrt{2AK_1}$. The expression II is useful in discussing the low frequency branch because of $|\omega/\gamma| = 2AK_1$ when $H = 0$. Expression I becomes indefinite for that case but II gives zero. Apart from the dependence of the ratio m_y/m_z on (ω/γ), H, and the temperature through a, one important feature appears.

The branch with $|\omega/\gamma| \leq \sqrt{2AK_1}$ represents a precession around the a-axis in a sense opposite to the sense of rotation in the paramagnetic state. According to section 1B, the ratio $m_y/m_z = ig_y/g_z$ in paramagnetism. Because the expression II is negative imaginary or zero for the whole branch, above remark is quite general. Experiments with circularly or better: elliptically polarized light might be carried out in order to prove that the sense of rotation in this branch is „anti-paramagnetic".

The branch with $|\omega/\gamma| \geq \sqrt{2AK_2}$ represents a precession around the a-axis in the same sense as in the paramagnetic state. This

is because expression I is positive imaginary for the whole branch.

H along a-axis and $< H_c^*$

	H	$\lvert\omega/\gamma\rvert$	m_y/m_z	H	$\lvert\omega/\gamma\rvert$	m_y/m_z
Low frequency branch	0	$\sqrt{2AK_1}$	$m_y = 0$	aH	$= \omega/\gamma$	-i
High frequency branch	0	$\sqrt{2AK_2}$	$m_z = 0$			

	H	$\lvert\omega/\gamma\rvert$	m_y/m_z
Low frequency branch	H_c^*	0	$m_z = 0$
High frequency branch	H_c^*	$[2AK_2 + 2AK_1(1+a+1/a)]^{1/2}$	$\dfrac{i(2AK_2+2AK_1/a)}{\omega/\gamma\sqrt{2AK_1/a}}$

When T = 0^o, m_y/m_z = 1.6 i for the high frequency branch and when T = 4.3^o this ratio is i. As will be proved at the end of this section, the absorption intensity equals zero when **h** points in a direction such that **m** = 0. This makes it clear why the normal modes already give some insight in the experiments.

The low frequency branch has been studied experimentally in Ch. IV where $H_{px} = (2/g_a)\lvert\omega/\gamma\rvert$ = 3050 Φ.

No resonance absorption was obtained when **h** was along the a-axis. The table shows that when $H = H_c^*$ one has $\omega/\gamma = 0$ and $m_z = 0$. When $aH = \omega/\gamma$ one has $m_y = -im_z$. This happens at a temperature of 2.9^oK. When $H = 0$ and $\omega/\gamma = 2AK_1$ one has $m_y = 0$. This happens at 4.1^oK.

Fig.3 Ch.IV shows that at low temperatures a h.f. field along the b-axis gives rise to the greatest energy absorption; at 2.9^oK both axis are about equally effective with respect to absorption and near 4^oK a h.f. field along the c-axis gives rise to energy absorption, while the b-axis is practically ineffective.

As a closing remark for this case, I would like to compare the conclusions with those obtained by Keffer, et al. [18] for the model of Kittel [15] with unaxial anisotropy. In their case a degeneracy for H = 0 exists and two modes of oscillation with $\lvert\omega/\gamma\rvert = H_c$ are possible. One of the modes represents a left- and the other a right-circularly polarized motion. When a field, **H**, is applied along the a-axis, one of the precessions will have the same sense of rotation as would be induced by the torque due to **H** alone. The frequency of this precession equals $\lvert\omega/\gamma\rvert = H_c + H$. For the other mode the sense of precession is antiparamagnetic and the frequency is given by $\lvert\omega/\gamma\rvert = H_c - H$.

In the orthorhombic case for $H = 0$ there are two modes of oscillation. The mode with the higher frequency represents an oscillation along the b-axis, which opens into an ellipse with

paramagnetic sense of rotation for increasing H. The mode with the lower frequency represents an oscillation along the c-axis, which opens into an ellipse with antiparamagnetic sense of precession for increasing H. The plane of rotation is the b c-plane, m_x being zero.

Instead of studying the motion of the sum vector, one can also ask what the motion of the magnetization vectors $\mathbf{M}^+$ and $\mathbf{M}^-$ will be. It follows from calculation that they precess in the paramagnetic sense for the high frequency branch, but the ellipse described by the + spins is somewhat larger than the ellipse described by the spins oriented in a direction opposite to $\mathbf{H}$. For the low-frequency branch the precession is antiparamagnetic and the ellipse of the – spins is the bigger one.

b) $H > H_c^*$. The normal mode equations can be obtained from (2.02) by putting $\mathbf{h} = 0$ and using the relation $\beta = 0$ and $\psi = \pi/2$. This leads to the following static quantities: $H_x = H$, $M_x = \chi_\perp H$, $M_y' = -2M_o$, and the other components are zero.

The determinant is thus reduced to: $m_y' = 0$ and to the product of two determinants, one of the second and the other of the third order.

The second order determinant describes the resonance at $\omega/\gamma = 2A(K_2-K_1)$ for all values of H higher than H_c^*. The only, linearly oscillating, components are m_z' and m_x. In this case, the horizontal line in fig.1 Ch.II, only high frequency radiation with $\mathbf{h}$ along the a-axis will be absorbed. This has actually been observed in the experiments of Ubbink e.a. [3].

The third order determinant gives the equation $(\omega/\gamma)^2 = H^2 - 2AK_1$. Here one has $m_x = 0$ and $m_y/m_z = \frac{iH}{|\omega/\gamma|}$. The precession of the sum vector is in the paramagnetic sense. At high fields and high temperatures $2AK_1$ becomes unimportant so that $|\omega/\gamma|$ approaches H, the motion approaching the paramagnetic precession.

In the case of this resonance a simple relation exists between the ratio of the absorption when $\mathbf{h}$ is along the b- or c-direction, ABH/ACH, and m_y/m_z, namely: ABH/ACH = $(m_y/m_z)^2$.

Another connection between the normal mode oscillation and the actually observed absorption arises from the fact that $\mathbf{h}$ in a certain direction k will not give rise to absorption, when m_k in that direction equals zero. The proof of this theorem is easily obtained as a result of the properties of equation of motion 2.02.

Writing this equation as $i(\omega/\gamma)\mathbf{m} = F(a\mathbf{m} + b\mathbf{m}') + [\mathbf{M} \times \mathbf{h}]$ one can find a certain direction k, in which the normal mode equation reads $i(\omega/\gamma)m_k = F'(am_1 + .. + m_1' + ..)$. Assuming that this expres-

sion equals zero, the resulting equation is $i(\omega/\gamma)m_k = [\mathbf{M} \times \mathbf{h}]$. This expression is always zero when $\mathbf{h} = h_k$, as had to be proved.

C. *Antiferromagnetic high frequency susceptibility*

In this section the case **H** parallel to the *a*-axis will be considered.

a) Low line, $H < H_c^*$. The six equations obtainable from (2.02) by substitution of the static values given in section 2Ba are:

$$
\begin{aligned}
& m_x = m_x' = 0 \\
& -(i\omega/\gamma + 1/t_y\gamma)m_y + Hm_z + K_2/M_o m_z' = \chi_{\parallel} H h_z \\
& -Hm_y - (i\omega/\gamma + 1/t_z\gamma)m_z - K_1/M_o m_y' = -\chi_{\parallel} H h_y \qquad (2.04) \\
& 2AM_o m_z - (i\omega/\gamma + 1/t_y\gamma)m_y' + \alpha H m_z' = 2M_o h_z \\
& -2AM_o m_y - \alpha H m_y' - (i\omega/\gamma + 1/t_z\gamma)m_z' = -2M_o h_y
\end{aligned}
$$

The anisotropy in the relaxation time t has been denoted by a subscript referring to the axes.

These equations has been solved for m_y and m_z by applying Cramer's rule, namely that $m_i = (a_1A_{1i} + a_2A_{2i} + \ldots a_6A_{6i})/|A|$, where $a_1 \ldots a_6$ are the right members of (2.04), A_{1i} is the cofactor of m_{1i} and $|A|$ stands for the determinant of the equations. One gets

$$
m_y = \chi_{\perp} h_y \frac{B\gamma^2}{N} \frac{1}{\omega_o^2 - \omega^2 + i\omega(1/t_y + 1/t_z)}
$$

$$
m_z = \chi_{\perp} h_z \frac{C\gamma^2}{N} \frac{1}{\omega_o^2 - \omega^2 + i\omega(1/t_y + 1/t_z)}
$$

B, C and N are given by:

$$
B = 2AK_2(2AK_1 - \omega^2/\gamma^2) - H^2\{\alpha 2AK_1 + (1-\alpha)(\alpha 2AK_2 - \alpha^2H^2 + \omega^2/\gamma^2)\}
$$

$$
C = 2AK_1(2AK_2 - \omega^2/\gamma^2) - H^2\{\alpha 2AK_2 + (1-\alpha)(\alpha 2AK_1 - \alpha^2H^2 + \omega^2/\gamma^2)\}
$$

$$
N = 2A(K_2 + K_1) + H^2(1+\alpha^2) - 2\omega^2/\gamma^2
$$

Notice that $B\gamma^2/N$ has the dimension of ω^2. Simplifying for the case of narrow lines in the way discussed in section 1C of this chapter one obtains the imaginary component of the antiferromagnetic h.f. susceptibility as

$$
\chi_z'' = \chi_{\perp}^f \frac{\omega_o \Delta\omega}{4(\omega_o - \omega)^2 + \Delta\omega^2}
$$

This equation is identical with the equation (1.19) for the paramagnetic susceptibility except for the following: Here one has $\chi_\perp$ and in the paramagnetic case χ_o. $\chi_\perp$ equals χ_o at the Néel temperature, because $\chi_\perp$ is a constant in the antiferromagnetic temperature region. Furthermore one has the dimensionless quantity $f = C\gamma^2/N\omega_o^2$, which equals 1 in the paramagnetic case. $\Delta\omega$ stands for $1/t_y + 1/t_z = \Delta\omega$, just as in (1.19).

A very simple calculation, giving a measurable quantity independent of $\Delta\omega$, was first made in order to test the theory. It was the calculation of the ratio $\chi_y''/\chi_z'' = (g_b/g_c)^2(B/C)$.

The symbols used in B and C have to be interpreted in the way pointed out in section 2A for the anisotropy of the g-factor.

One obtains:

$$\frac{\chi_y''}{\chi_z''} = \frac{g_b^2\,\alpha H_b^{*2}(\alpha H_c^{*2} - H_{px}^2) - H^2\{\alpha^2 H_c^{*2} + (1-\alpha)(\alpha^2 H_b^{*2} - \alpha^2 H^2 + H_{px}^2)\}}{g_c^2\,\alpha H_c^{*2}(\alpha H_b^{*2} - H_{px}^2) - H^2\{\alpha^2 H_b^{*2} + (1-\alpha)(\alpha^2 H_c^{*2} - \alpha^2 H^2 + H_{px}^2)\}} \qquad (2.05)$$

The quantities occurring in this expression are all known in their temperature dependence from the measurements described in Chapter I and II, while $H_{px} = 3050$ Φ.

As has been derived in section (4.02) Ch.IV, the experimental value A is proportional to χ'', so that:

$$\frac{\chi_y''}{\chi_z''} = \frac{ABL}{ACL}$$

This ratio was calculated as a function of temperature and has been plotted as the theoretical curve in Ch.IV fig.3. The experimental points represent the ratio between A_{peak} when $\mathbf{h} = h_y$, ABL, and A_{peak} when $\mathbf{h} = h_z$, ACL. Within the experimental error there is agreement between theory and experiment. Some interesting features are: At 4.07°K one has $H_{px}^2 = H_c^{*2}$ and $H = 0$, so that ABL equals zero. With decreasing temperature ABL increases so that at 2.9°K, when $H_{px} = \alpha H$ one has ABL/ACL = $(g_b/g_c)^2$. At still lower temperatures ABL becomes greater than ACL. It may be remarked that qualitatively the same picture was suggested in the preceding section by the study of the normal mode.

It has been observed experimentally that A_{peak} (ab-plane)= = ABL $\sin^2\zeta_b$, where ζ_b is the angle between **h** and the a-axis in the ab-plane. This is easily understandable now, because $\chi_x'' = 0$ and A is proportional to h^2 (1.11). The only effective component of **h** is $h\sin\zeta_b$, so that A will be proportional to $\sin^2\zeta_b$. The same is true for the intensity in the ac-plane and its dependence on ζ_c, in accordance with the experiments of Ch.IV sect.3.

Another calculation has been carried out, namely for χ_z'' = ACL as a function of temperature. This time, however, the variation

of $\Delta\omega$ with temperature must be included. As will be described in Ch.V, the experimentally observed linewidth was obtained by plotting A vs. H, thus giving ΔH_L. Because H vs. ω is known, it was possible to compute $\Delta\omega/\gamma = \frac{\Delta\omega}{\gamma\Delta H_L}\Delta H_L = \Delta H_{Lpx}$ vs. T in Ch.V fig.3b. Although the experimental shape of the resonance curve is not Lorentzian and even not symmetrical, contrary to what follows from the theory developed here, the ΔH_{Lpx} values, combined with the values of C and N as functions of temperature, gave a good description of the measured intensities.

The theoretical curve ACL vs. T in Ch.IV fig.4 has been calculated with $\chi''_{z_{peak}} = (g_c/2)^2\,\chi_\perp \frac{C}{H_{px}^2 N}\frac{H_{px}}{\Delta H_{Lpx}}$ as can easily be obtained from the expression for χ''_z by putting $\omega = \omega_0$.
The factor $f = C/H_{px}^2 N$ equals 0.93 and $\Delta H_{Lpx} = 33$ Φ at T = 1.35°K. This gave as a result $\chi''_z = 110\,\chi_\perp$ at that temperature. In the same way χ''_y has been calculated at 1.35°K, resulting in $\chi''_y = 157\chi_\perp$. The theorerical values ABL and ACL at 1.35°K are thus:
ABL = k.157 $\chi_\perp$, in which the proportionality constant, k, equals
ACL = k.110 $\chi_\perp$ $4\pi\,Q_o/V$ according to Ch.IV (4.02).

The theoretical ACL vs. T curve, plotted in fig.4 Ch.IV has been calculated with: ACL = k.χ''_z(peak) in which for conveniency sake k = $1/(100\,\chi_\perp)$ has been inserted and the temperature dependence of C, N and ΔH_{Lpx} was taken into account.

An interesting feature of the theory is, that a prediction can be made of the intensity of the paramagnetic absorption as compared with the antiferromagnetic absorption. At a temperature just above 4.3°K, the substance is paramagnetic and the susceptibility can be described by $\chi''_{z,p} = (g_c/2)^2\chi_\perp\frac{H_{px}}{\Delta H}$ resulting from (1.19). The measurements on the paramagnetic resonance have been done at 20° and 80°K, giving a $\Delta H \equiv \Delta H_{px} = 80$ Φ. Because the relationship between the static susceptibilities at different temperatures is given by the Curie-Weiss law in the way discussed in Ch.IV, it is possible to derive theoretical values for the absorption intensity at 20° and 80°K. The hypothetical $\chi''_{z,p}$ at 4.3°K equals $45\chi_\perp$ when $\Delta H = 80$ Φ is introduced in (1.19). It then follows that at 20°K, where a $\Delta H = 80$ Φ has actually been measured one can write $\chi''_{z,p} = 45\chi_\perp(4.3+5)/(20+5) = 16\chi_\perp$ so that AC PM 20°K was plotted as 0.16 in the theoretical column of Ch.IV section 3δ.

b) High line, $H > H_c^*$. The six equations obtainable from (2.02) by the introduction of the static values given in section Bb are:

$$m'_y = 0$$

$$-(i\omega/\gamma+1/t_x\gamma)m_x + (K_2 - K_1)/M_o m'_z = 0$$

$$-2AM_o m_x - (i\omega/\gamma+1/t_z\gamma)m'_z = -2M_o h_x$$

These equations will be called "ridge" eq

$$-(i\omega/\gamma+1/t_y\gamma)m_y + Hm_z = \chi_\perp H h_z$$

$$-Hm_y - (i\omega/\gamma+1/t_z\gamma)m_z + K_1/M_o m'_x = -\chi_\perp H h_y$$

$$2AM_o m_z - (i\omega/\gamma+1/t_x\gamma)m'_x = 2M_o h_z$$

The solution of what I called the "ridge" equations is very simple. Here one obtains $\chi_y = \chi_z = 0$ and

$$\chi_x = (g_a/2)^2 \chi_\perp \frac{\omega_o^2}{\omega_o^2 + (i\omega+1/t_x)(i\omega+1/t_z)}$$

a formula nearly identical with (1.19) for paramagnetic resonance. The difference from paramagnetic resonance is evident, however. In paramagnetic resonance only a h.f. magnetic field perpendicular to the static field will give rise to absorption, while here only a h.f. field *in the direction* of the static field will be absorbed. The resonance is independent of the value of the magnetic field and occurs at a frequency $\omega/\gamma = \sqrt{2A(K_2 - K_1)}$. This resonance is denoted by the horizontal line in fig.1 Ch.II.

One obtains as $\chi''_{x_{peak}} = (g_a/2)^2 \chi_\perp \frac{\omega_o}{\Delta\omega}$.

The other three equations define the relation between ω/γ and H as: $H^2 = 2AK_1 + (\omega/\gamma)^2$. This resonance was called the high line resonance and it was observed at about 7200 Φ in the temperature region $1.2^o - 2.3^o$K (see Ch.III). Solving the equations one obtains

$$\chi''_y = (g_b/2)^2 \chi_\perp \frac{H^2}{H_{px}^2} \frac{\omega\Delta\omega}{4(\omega_o-\omega)^2 + \Delta\omega^2}$$

where $\Delta\omega$ stands for

$$\Delta\omega = 1/t_z + H^2/H_{px}^2 t_y - \alpha H_c^{*2}/H_{px}^2 t_x$$

which becomes $\Delta\omega = 1/t_z + 5.6/t_y - 4.5/t_x$

when the values of H, H_{px} and αH_c^{*2} at 1.35^oK are introduced.

It may be remarked that the high line resonance approaches the paramagnetic resonance in many aspects for high frequencies so that $H_{px}^2 >> \alpha H_c^{*2}$. This condition is also fulfilled for high *temperatures*, but there one encounters the complication that the resonance does not exist any longer, the resonance occurring at $H = H_c^*$ instead (orientation resonance).

The following expressions represent that paramagnetic tendency:

Resonance condition. $H_H^2 = H_{px}^2 + \alpha H_c^{*2}$

Normal mode behaviour. $m_y/m_z = (g_b/g_c) iH/H_{px}$ (Section Bb).

Linewidth formula. $\Delta\omega = \frac{1}{t_z} + \frac{H^2}{H_{px}^2}\frac{1}{t_y} - \frac{\alpha H_c^{*2}}{H_{px}^2}\frac{1}{t_x}$

For very high frequencies the strange, negative, t_x term is negligible.

In the expression for $\Delta\omega$ the relaxation time in the direction of the alignment, t_y, plays a role, contrary to the case of the low line, where the corresponding t_x does not appear in the equation.

For a possible explanation of the conspicuous broadening of the high line with decreasing temperature, one could imagine that t_y would decrease with decreasing temperature, and would become predominant in the expression for $\Delta\omega$.

Following from the resonance condition for this line, one gets

$$\chi''_{y_{peak}} = (g_b/2)^2 \chi_\perp \frac{H}{\Delta H} \quad \text{and} \quad \chi''_z = (g_c/2)^2 \chi_\perp \frac{H_{px}^2}{H\Delta H}$$

where ΔH is the actually measured linewidth as plotted in fig.7 Ch. V. The formula predicts ABH/ACH = $(g_b/g_c)^2 (H/H_{px})^2 = 4.6$ as compared with 4 (± 1), the experimental value at 1.35°K (Ch.IV).

In good agreement with the large linewidth at low temperature, is the relatively weak peak absorption. Taking $\Delta H = 250$ Φ at 1.35°K one obtains $\chi''_{y_{peak}} = 30\,\chi_\perp$ and $\chi''_{z_{peak}} = 6.5\,\chi_\perp$, giving the values ABH = 0.30 and ACH = 0.065 in the theoretical column of Ch.IV section δ (see section a), high line. It is clear that the intensity should depend on $\sin^2\zeta$ (b or c) for the same reasons as for the low line, because $\chi''_x = 0$. This dependence was actually measured.

c) Orientation resonance, $H = H_c^*$ (see also Ch.II).

The equation for the normal modes can be treated as a special case of the more general problem: to find the equations for the case that **H** lies in the *ab*-plane and the spins make an angle ψ with the *a*-axis. In the case of the orientation resonance the equations of the following section, D, can be used if one inserts: $H = H_c^*$ and $\beta = 0$.

The resonance condition is obtained by putting the determinant of the equations equal to zero, thus giving ω/γ as a function of ψ. ψ can have all values between 0 and $\pi/2$, which gives rise to a range of ω/γ values at which resonance occurs for $H = H_c^*$, the so called orientation resonance.

The six equations are rather complicated and are not seperable into smaller groups. As is shown in section D for the general case one obtains: The motion of m is elliptical, one of the main axes being the z-axis, the other axis lying in the ab-plane. This means that the motion is linearly polarized in the ab-plane, because m_x/m_y is real. The a-axis is now also effective with respect to absorption. It can be proved that at high temperatures the main axis of the ellipse, that lies in the ab-plane, shifts towards the a-axis, so that at $4.2^{O}K$, where $(\omega/\gamma)^2 = 2A(K_2-K_1)$, the main axis is oriented along the a-axis, resulting in the case of the "ridge" equations.

D. *Theoretical interpretation of the nodal line experiments*

The physical situation is the following: A static magnetic field, **H**, can be applied in any direction in the ab-plane. The angle between this field and the a-axis will be called β. Under the influence of this field the spins will take in a position with respect to the a-axis, characterized by the angle ψ, the angle between $\mathbf{M}'$ and the a-axis.

In addition to the static field, a h.f. magnetic field can be applied independently of the static field. (See Ch.IV). The angle between this h.f. field and the a-axis will be called ζ. For each β a value of $\zeta = \eta$ exists, the so called nodal angle, for which the intensity of the absorption is zero. In order to obtain the relation between β and η the equations for the oscillation of **m** in the normal modes will be solved. It will turn out, that m_x and m_y are in phase with each other, while m_z is $\pi/2$ out of phase with m_x and m_y. This implies that the oscillation in the ab-plane is linear, so that it makes sense to define an angle θ between the a-axis and the direction of the oscillation of **m** in the ab-plane. When a h.f. field is applied in a direction perpendicular to the normal mode vibration in the ab-plane, no absorption will result according to a theorem derived in section B. This makes it clear that $\eta = (\theta - \pi/2)$, so that $-\mathrm{tg}\eta = \mathrm{cotg}\theta = m_x/m_y$.

The equations necessary for the calculation of this ratio can be obtained from (2.02) in the usual way by putting $\mathbf{h} = 0$ and omitting the damping terms. The static quantities occurring in the formula are given in (2.03). This leads to the following equations, which are formulae 12 of Yosida [6].

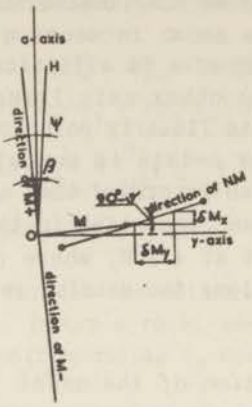

Fig. 1. Normal mode oscillation for the low line.

$$\frac{-i\omega}{\gamma}m_x \qquad -H\sin\beta m_z \qquad +\frac{K_2-K_1}{M_o}\sin(\psi-\beta)m'_z=0$$

$$\frac{-i\omega}{\gamma}m_y+H\cos\beta m_z \qquad +\frac{K_2}{M_o}\cos(\psi-\beta)m'_z=0$$

$$H\sin\beta m_x \qquad -H\cos\beta m_y\frac{-i\omega}{\gamma}m_z+\frac{K_1}{M_o}\sin(\psi-\beta)m'_x \qquad -\frac{K_1}{M_o}\cos(\psi-\beta)m'_y \qquad =0$$

$$2AM_o\sin(\psi-\beta)m_z \qquad -\frac{i\omega}{\gamma}m'_x \qquad +\alpha H\cos\psi\sin(\psi-\beta)m'_z=0$$

$$2AM_o\cos(\psi-\beta)m_z \qquad -\frac{i\omega}{\gamma}m'_y+\alpha H\cos\psi\cos(\psi-\beta)m'_z=0$$

$$-2AM_o\sin(\psi-\beta)m_x-2AM_o\cos(\psi-\beta)m_y-\alpha H\cos\psi\sin(\psi-\beta)m'_x-\alpha H\cos\psi\cos(\psi-\beta)m'_y-\frac{i\omega}{\gamma}m'_z=0$$

Now: $\cos\theta = m_x/m_y = -(g_a A_{31}/g_b A_{32})$

where A_{31} and A_{32} stand for the respective minors of m_x and m_y. The calculation gives

$$A_{31} = -(\omega/\gamma)^2 H[\sin\beta\{\alpha^2H^2\cos^2\psi - (\omega/\gamma)^2\} + \alpha 2A(K_2-K_1)\cos\psi\sin(\psi-\beta)+$$
$$+\cos(\psi-\beta)\{2AK_2\sin\psi - 2AK_1\cos\beta\sin(\psi-\beta)\}]$$

$$A_{32} = -(\omega/\gamma)^2 H[\cos\beta\{\alpha^2H^2\cos^2\psi - (\omega/\gamma)^2\} - \alpha 2AK_2\cos\psi\cos(\psi-\beta) +$$
$$+\sin(\psi-\beta)\{2AK_2\sin\psi - 2AK_1\cos\beta\sin(\psi-\beta)\}]$$

The frequency, ω, appearing in this ratio must satisfy the condition that the determinant equals zero. It is the resonance frequency, studied by Ubbink and Yosida. In Ch.III an analysis is

made of the resonance field **H** as a function of β in the ab-plane, at a value ω corresponding to a frequency of 9500 MHz. Another analysis is made in Ch.III of ψ as a function of β. The values for **H** and ψ used in the calculation of θ have been taken from the theoretical curves fig.1 and fig.2 Ch.III. In this way $(\theta - \pi/2)$ has been calculated as a function of β and its value has been plotted as the theoretical curve in fig.5 Ch.IV. The corrections due to the anisotropy of the g-value have been taken into account and the calculation was carried out with: $T = 1.4^{o}K$; $\alpha H_c^{*2} = 41.5$; $\alpha H_b^{*2} = 123.8$; $\alpha = 0.96^5$; $g_a/g_b = 1.07$; $H_{px} = 3.12$; $H_\beta = (g_\beta/2)H_{res}$, where H_{res} was taken from Ch.III fig.2, and

$$g_\beta = \sqrt{(g_a \cos\beta)^2 + (g_b \sin\beta)^2}$$

It may be remarked that for small values of β, A_{31} becomes very small. Two different situations can be distinguished.

$H_{res} < H_c^*$, the low line. Now ψ is very small too, so that θ comes out to be nearly $+\pi/2$. This situation is sketched in fig.1.

$H_{res} > H_c^*$, the high line. ψ is almost $\pi/2$ and θ comes out to be nearly $-\pi/2$ radian. Summarizing for small β: For the low line η is a small negative angle and for the high line η is nearly π radian, in accordance with the sketch in Ch.IVb.

It is instructive to study the problem of the nodal line for the case of very low frequency. In order to avoid the orientation resonance and to simplify the formulae, it will be assumed in addition, that the temperature is so low, that α may be considered to be 1. In that case the resonance diagram in the ab-plane shall contract, so that resonance only occurs when the static magnetic field is applied parallel or nearly parallel to the a-axis, at values slightly above and below H_c^*. There is a continuous change of ψ from 0 ($\beta = 0$, $H < H_c^*$) to $\pi/2$ radian ($\beta = 0$, $H > H_c^*$) along the resonance diagram. The calculation for that case, taking $\omega/\gamma \ll H$ and $\beta \ll \psi$, gives: $\mathrm{tg}2\psi = \mathrm{cotg}\theta$. Here ψ has to be considered as a negative angle when β is taken as a positive angle (fig.1). One finally obtains for this case the relation $\eta = 2\psi$, a relation which gives already a qualitative description of the nodal line experiments at 9500 MHz. The relation means that the oscillation of the spins in the ab-plane is perpendicular to a line which makes the same angle with the spin-direction as the spin-direction makes with the a-axis.

Chapter VII

SEARCH FOR NEW ANTIFERROMAGNETIC MATERIALS

1. Introduction

A short survey is given of recent measurements on paramagnetic resonance in several concentrated salts. The experiments were carried out in an attempt to find new antiferromagnetic substances with Néel temperatures in the liquid helium or hydrogen temperature range. Most of the following salts have been studied as single crystals: $Cu(NH_3)_4SO_4.H_2O$; $CuBr_2$.aq.; $CoCl_2.6H_2O$;; $FeCl_3$; $MnCl_2.4H_2O$ and $MnBr_2.4H_2O$; UI_3.

2. Experimental method

The same apparatus as has been described in chapter IV for experiments at 9400 MHz has been used.

3. Results

a. $Cu(NH_3)_4SO_4.H_2O$. This substance has been investigated, because room temperature measurements at 21000 MHz. gave results very similar to those obtained for $CuCl_2.2H_2O$ [25].

The technique of the preparation of big single crystals was developed by M.Garber, while useful chemical information was obtained from Mr. F.Dolle of the inorganic laboratory. A detailed description of the method will be published in a forthcoming paper.

It was found that the crystal symmetry was orthorhombic, with g-values 2.045 and 2.145 along the principal axes in a plane perpendicular to the long axis of the crystal.

When the magnetic field was directed along the crystal axis characterized by $g = 2.045$, the following values for the linewidth were obtained:

T	$\Delta H_{½}$	Peak absorption = A	A × T × $\Delta H_{½}$
80°K	35 Φ ± 5	0.06	150
20.5°		0.27	160
15°		0.36	140
4.2°	50 Φ ± 2	0.34	
3.2°		0.35	55
2.2°		0.29	
2.1°	100 Φ ± 10	0.25	
2.0°	160 Φ ± 10	0.26	52
1.4°		0.22	50

The linewidth starts increasing at about 3°K, and at the same temperature the intensity of the peak of the absorption line starts decreasing. Assuming the product of these, effectively the area under the resonance line, to be proportional to the susceptibility, it is interesting that this product is inversely proportional to the temperature below 4°K, as is shown in the last column. This is also true between liquid hydrogen and liquid air temperatures, but the respective proportionality constants differ by a factor of three. It is not certain whether this is a real effect or an effect due to experimental imperfection, as the two regions were measured in different runs.

b. Copper bromide hydrate. These crystals were obtained by a slow evaporation of a saturated solution of copper bromide in water at room temperature. The solid phase that came out of solution consisted of black needles of $CuBr_2$, together with a small amount of blue-green crystals, the hydrate.

The crystals were of orthorhombic symmetry and the g-values along two of the principal axes were: 2.185 and 2.275. Linewidth measurements were done along the axis characterized by $g = 2.185$, and the results are given in the table.

T	$\Delta H_{½}$
80°K	55 Φ
20°	60
14°	90
4°-1.3°	120

Here the linewidth was constant within the experimental error in the temperature region of liquid helium.

The quantity A × T × $\Delta H_{½}$ was not a constant in the region of 4°K – 1.3°K, but decreased with decreasing temperature. There was no indication from the lineshape, that the broadening was due to the beginning of a structure.

The line had the typical peaked shape of exchange narrowed salts.

After this rather negative result, a literature study has been made of the hydrates of the copper halogens.

$CuCl_2$ and $CuBr_2$ have been studied by means of x-rays and it was found [31], that both had the same crystal structure. The respective Néel temperatures are [24]: 70°K and 193°K, indicating that the exchange forces are greater in the bromide than in the chloride. While the stable hydrate of $CuCl_2$ is the di-hydrate, the corresponding compound of $CuBr_2$ does not exist, but a rather stable tetrahydrate is formed instead [29]. By evaporating a saturated aqueous solution of $CuBr_2$ below 15°C, the solid phase consists of blue green crystals of $CuBr_2.4H_2O$, but above 20°C, the solid phase consists of black rhomboids of $CuBr_2$. At 18°C the two solid phases are in equilibrium with the solution. Most likely the tetrahydrate is magnetically too diluted to give a Néel point above 1.3°K. CuI_2 is a very unstable substance, but it might be interesting to study the CuF_2, because it forms a dihydrate.

c. $CoCl_2.6H_2O$. The crystals were obtained by crystallizing $CoCl_2$ from an aqueous solution and were ruby-red. No paramagnetic resonance could be detected at 80°K and 20°K; perhaps the line was too broad at these temperatures, a property that is typical for cobalt salts and is ascribed in these cases to the strong coupling of the spin with the lattice by the unquenched orbitals.

d. Ferric chloride. According to the literature [24], the Néel temperature of $FeCl_3$ should be equal or less than 11.5°K. Measurements on a powder of $FeCl_3$ did not show interesting changes in the temperature range of 20°-10°K.

The linewidth at 20°K and 10°K was 250 Φ and the g-factor 2.21.

e. $MnBr_2.4H_2O$ and $MnCl_2.4H_2O$

The paramagnetic region. Both substances gave broad paramagnetic lines with linewidths of 1000 – 3000 Φ and $g = 2.0$.

In studies on $MnBr_2.4H_2O$ it was found, that the linewidth depended strongly upon the orientation of the h.f. field relative to the crystal axes, while the direction of the external field was less important. This would make a further study on the paramagnetic behaviour of these substances very desirable.

The great linewidth in these substances, where exchange narrowing should be appreciable, must be due to the contribution of the crystalline field and the magnetic moment of the nuclear spin of manganese. These effects give rise to respectively a fine structure and a hyperfine structure of 30 lines, in total with a distance of the order of 1500 Φ between the extreme lines, in diluted magnanese salts [30].

The antiferromagnetic region. The Neel temperature of $MnCl_2.4H_2O$ equals 1.62^oK [27], and of $MnBr_2.4H_2O$ [26]: 2.2^oK.

Resonance measurements in $MnCl_2.4H_2O$ at 9400 MHz down to 1.3^oK did not show striking effects, but in the bromide great changes occurred in the resonance diagram. When going down in temperature, the paramagnetic line, with linewidth of about 2000 Φ, did not disappear, and its intensity increases with decreasing temperature. In addition to this line there appeared other lines and a picture at 1.3^oK, with the external magnetic field along the direction preferred by the spins, is given. It may be remarked, that it is possible to "cut out" the "paramagnetic" line, by orienting the h.f. field parallel to the external magnetic field. This suggests that polarization measurements might be interesting here as well.

The experiments are still in the first stage, but it is nevertheless certain, that in $MnBr_2.4H_2O$ an interesting substance has been found for further antiferromagnetic resonance studies.

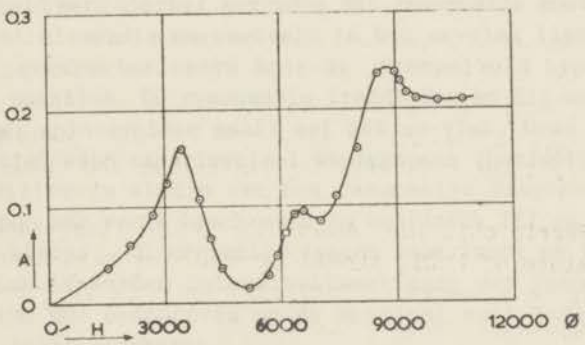

Fig. 1. Antiferromagnetic resonance in $MnBr_2.4H_2O$ at 1.3^oK with the external magnetic field along the preferred axis.

f. UI_3. It is known from other measurements, that this substance has a Néel temperature of 3.2^oK [32]. The substance was prepared in the laboratory of inorganic chemistry under the supervision of Mr. F.Dolle. It was obtained as an orange brown powder by heating Uranium powder and Iodide together for several hours [33].

The substance was hygroscopic and reacted slowly with the oxygen from the air. It was therefore kept in an atmosphere of nitrogen. A broad resonance line with small peak intensity was obtained at 80^oK, and the g-factor was slightly smaller than 2.

It would be interesting to grow single crystals of this substance, perhaps by slow sublimation from the vapor, and study the resonance at liquid helium temperature.

4. Final remarks

In chapter IV it was remarked that the intensity of the free radical diphenyl-trinitrophenyl-hydrazine-benzene was practically constant below $4^{o}K$, while its linewidth increased with decreasing temperature and this behaviour was also found in the two copper salts described in sections a. and b. of this chapter. However, in the substance: a, the intensity was still increasing with decreasing temperature, and it might be a sign of the onset of antiferromagnetism at still lower temperatures. Such an effect has indeed been observed in the resonance of MnF_2 [28] with a Néel temperature of $70^{o}K$, where the approaching of the Néel temperature from high temperatures was manifested by a broadening of the paramagnetic resonance line and a decrease of its peak intensity.

SAMENVATTING

> ---- en zag met helse ontzetting wat dat gedruis als van hollende schreden veroorzaakt had; want achter de tralies van het geleidelijk zakkende hek stond de manshoge, zwartglanzende, spin.
>
> *Havank. De weduwe in de wilgen*

Het doel van de onderzoekingen, verzameld in dit proefschrift, was de experimenten van Ubbink e.a. over de antiferromagnetische resonantie in koperchloride-hydraat uit te breiden en de bestaande theorieën van Ubbink, Nagamiya en Yosida verder te ontwikkelen.

Daartoe zijn metingen verricht bij zeer hoge frequenties (hoofdstuk I) en werd de theorie hierop toegepast (hoofdstuk II). Als bijzonderheid werd hierbij gevonden dat resonantie moet optreden wanneer het uitwendig magneetveld in het *ac*-vlak ligt en een waarde heeft, gekarakteriseerd door de „drempelveld hyperbool" van Gorter en Haantjes. De resonantie treedt dan op bij een zekere hoek die het spin-systeem maakt met het *ac*-vlak. Deze „orientatie resonantie" werd experimenteel waargenomen (hoofdstuk I).

Een gedetailleerde studie van het resonantie diagram in het *ab*-vlak bij 9500 MHz wordt beschreven in hoofdstuk III en gewezen wordt op de – kleine – discrepantie tussen experiment en theorie.

In hoofdstuk IV worden intensiteitsmetingen der resonantielijnen bij 9400 MHz beschreven en de speciaal voor deze studie ontworpen trilholte geschetst.

Hoofdstuk V bevat lijnbreedte metingen bij 9400 MHz en een methode om nauwkeurig smalle lijnen te meten wordt beschreven.

Het bleek mogelijk een theorie te ontwikkelen, die goed rekenschap geeft van de waargenomen intensiteiten. Deze theorie, geschetst in hoofdstuk VI, berust op het model der moleculaire veldtheorie, waarin de spin-vectoren in twee subroosters verdeeld worden en dan gesommeerd tot twee macroscopische, tegengesteld gerichte, spins. In dit beeld werd het hoogfrequent magnetisch veld als storing op het statisch veld ingevoerd en dempingstermen toegevoegd, analoog aan de behandeling van het paramagnetisch geval door F.Bloch.

In hoofdstuk VII wordt een samenvatting gegeven van metingen, die tot doel hadden antiferromagnetische resonantie te bestuderen in andere stoffen. Een der onderzochte verbindingen, het mangaanbromide tetrahydraat, leek veelbelovend voor verdere studie.

REFERENCES

1. Poulis,N.J., van den Handel,J., Ubbink,J., Poulis,J.A., and Gorter,C.J., Phys.Rev.(2) **82** (1951) 552.
2. Ubbink,J., Poulis,J.A., Gerritsen,H.J., and Gorter,C.J., Commun. Kamerlingh Onnes Lab., Leiden, No.288d; Physica **18** (1952) 361. and Commun.293; Physica **19** (1953) 928.
3. Ubbink, J., Thesis 1953 Leiden.
4. Ubbink,J., Commun.Suppl.105b,c; Physica **19** (1953) 9; 919. Phys.Rev. (2) **86** (1952) 567.
5. Gorter,C.J., and Haantjes,J., Commun.Suppl.104b; Physica **18** (1952) 285.
6. Yosida,K., Progr.Theor.Phys. **7** (1952) 425.
7. Nagamiya,T., Progr.Theor.Phys. **11** (1954) 309.
8. Hardeman,G.E.G., and Poulis,N.J., Commun 300c; Physica .. (1955)
9. Hutchisson,C.A., Rutgers University, conference Oct.1951. Gerritsen,H.J., Okkes,R., Gijsman,H.M., and van den Handel,J., Commun.294c; Physica **20** (1954) 13.
10. Itoh,J., Fujimoto,M., and Ibamoto,H., Phys Rev **83** (1951) 852.
11. Van den Handel,J., Gijsman,H.M., and Poulis, Commun.290c; Physica **18** (1952) 862.
12. Poulis,N.J., and Hardeman,G.E.G., Commun.294a; Physica **20** (1954) 12.
13. Poulis,N.J., Thesis 1952 Leiden.
14. Van der Marel,L.C., van den Broek,J., Wasscher,J.D., and Gorter,C.J., Commun. ; Physica (1955)
15. Kittel,C., Phys.Rev.(2) **82** (1951) 565. See also Keffer,F., and Kittel,C., Phys.Rev. **85** (1952) 329.
16. Yosida,K., Progr.Theor.Phys. **7** (1952) 25.
17. Nagamiya,T., Progr.Theor.Phys. **6** (1951) 350.
18. Keffer,F., Kaplan,H., and Yafett,Y., Am.Journ.Phys. **21** (1953) 250.
19. Bloch,F., Phys.Rev. **70** (1946) 460.
20. Pake,G.E., Am.Journ.Phys. **18** (1950) 438.
21. Bleaney,B., and Stevens,K.W.H., Rep.on Progress (1953).
22. Van Vleck,J.H., and Weisskopf,V., Rev.Mod.Phys. **17** (1954) 229. Van Vleck,J.H., Phys.Rev. **74** (1948) 1168.
23. Penrose,R.P., Proc.Royal Soc.A, **62** (1949) 664.
24. Nagamiya,T., Advances in Phys. **13** (1955).
25. Okamura,T., and Date,M., Phys.Rev. **94** (1954) 315.
26. Henry,W.E., Phys.Rev. **90** (1953) 492 and **94** (1954) 1146.
27. Friedberg,S.A., and Wasscher,J.D., Commun.293c; Physica **19** (1953) 1072.

28. Maxwell,L.R., and McGuire,T.R., Rev.Mod.Phys. **25** (1953) 279.
29. Carter,S.R., and Megson,N.J.L., Journ.Chem.Soc. (1928) 2954.
30. Bleaney, B., and Ingram,D.J.E., Proc.Royal Soc.A, **205** (1951) 340.
31. Helmholz,L., Journ.Am.Chem.Soc. **69** (1947) 886.
32. Roberts,L.D., Lavalle,D.E., and Erickson,R.A. Journ.Chem.Phys. **6** (1954) 1145.
33. Katz,J.J. and Rabinowitch,E., The chemistry or Uranium I. National Nuclear Energy Series VIII – 5 page 533-536.
34. Frölich, H., Nature **157** (1946) 478.

STELLINGEN

I

De door Van Vleck gegeven formule voor de splitsing van het viervoudig ontaarde grondniveau in chroom-aluinen is onjuist.

J.H.Van Vleck, J.Chem.Phys. 7 (1939) 71

II

De door Nagamiya voorgestelde benaming van „resonance hyperbola" voor de resonantie figuur in het ac-vlak is aanvechtbaar.

T.Nagamiya, Progress of Theor. Phys. 11 (1954) 318

III

Het feit dat bij koperbromide-hydraat geen antiferromagnetisme is gevonden, dit in tegenstelling tot koperchloride-hydraat, dient hoogstwaarschijnlijk toegeschreven te moeten worden aan de grotere magnetische verdunning van eerstgenoemde stof.

Dit proefschrift, hoofdstuk VII

IV

Bij het opgeven van de breedte van een paramagnetische resonantielijn, kan het noodzakelijk zijn om, behalve de richting van het constant magneetveld t.o.v. de kristalassen, ook de richting van het h.f. magneetveld te vermelden.

R.Lacroix, Helv.Phys.Acta 27 (1954) 283.
B.Bolger, Conf. Paris No 146, 1955

V

De opmerking van Nagamiya betreffende de exciteerbaarheid van antiferromagnetische absorptie is onjuist.

T.Nagamiya,
K.Yosida, R.Kubo. Advances in Physics, IV (1955), 46

VI

Bij de studie van complexe verbindingen dient men naast de röntgenologische methode aandacht te besteden aan de mogelijkheid van resonantie experimenten.

VII

De motieven waarop Katz en Rabinowitch besluiten tot het bestaan van U_2C_3 zijn niet overtuigend.

J.J.Katz en E.Rabinowitch. The chemistry of Uranium I.
M.W.Mallett, A.F.Gerds and H.R.Nelson. J.Electrochem.Soc

VIII

Het zou aanbeveling verdienen dat de Nederlandse chemische industrie bij de naamgeving van haar producten het Latijn afschaft of tenminste de chemische formules toevoegt.

IX

Ter bestudering van phase-diagrammen in antiferromagnetische stoffen zouden metingen der soortelijke warmte van eenkristallen in magneetvelden waardevolle gegevens kunnen verstrekken.

T.van Peski-Tinbergen and C.J.Gorter. Physica 20 (1954) 592

X

De wijze waarop in de Koninklijke Nederlandse Landmacht de geestelijke verzorging van de militair plaats vindt, dient te worden herzien.

XI

Het verdient aanbeveling het dragen van veiligheidsbanden, zoals deze ook in vliegtuigen gebruikt worden, voor inzittenden van personenauto's wettelijk verplicht te stellen.

Saturday Evening Post, July (1955)

XII

Er dient naar gestreefd te worden het formaat van potten en flessen voor huishoudelijk gebruik zo veel mogelijk te normaliseren, teneinde vrije inwisselbaarheid te bevorderen.